1

The jamming scenario— an introduction and outlook

Andrea J. Liu[1], Sidney R. Nagel[2], Wim van Saarloos[3], and Matthieu Wyart[4]

[1] Department of Physics and Astronomy, UnivModeersity of Pennsylvania, Philadelphia, PA 19104, USA ajliu@physics.upenn.edu
[2] James Franck Institute, The University of Chicago, Chicago, IL 60637, USA srnagel@uchicago.edu
[3] Instituut-Lorentz, LION, Leiden University, P.O.Box 9506, 2300 RA Leiden, The Netherlands saarloos@lorentz.leidenuniv.nl
[4] Physics Department, New York University, 4 Washington Place, New York, NY 10003, USA mwyart@Princeton.edu

Abstract. The jamming scenario of disordered media, formulated about 10 years ago, has in recent years been advanced by analyzing model systems of granular media. This has led to various new concepts that are increasingly being explored in in a variety of systems. This chapter contains an introductory review of these recent developments and provides an outlook on their applicability to different physical systems and on future directions. The first part of the paper is devoted to an overview of the findings for model systems of frictionless spheres, focussing on the excess of low-frequency modes as the jamming point is approached. Particular attention is paid to a discussion of the cross-over frequency and length scales that govern this approach. We then discuss the effects of particle asphericity and static friction, the applicability to bubble models for wet foams in which the friction is dynamic, the dynamical arrest in colloids, and the implications for molecular glasses.

1.1 Introduction

Just over ten years ago it was proposed [1] to approach disordered condensed-matter systems in a more unified way than is usually done, by starting from the observation that many systems — not just molecular glasses, but also many soft-matter systems like granular media, colloids, pastes, emulsions, and foams — exhibit a stiff solid phase at high density, provided the temperature and the external forces or stresses are small enough. This proposal led to the idea of a *jamming phase diagram* for particulate systems, redrawn in Fig. 1.1.

The very idea that there would be a generic jamming phase diagram is less trivial than may appear at first sight, since granular media, emulsions and foams are in fact *athermal* systems — they are represented by points in

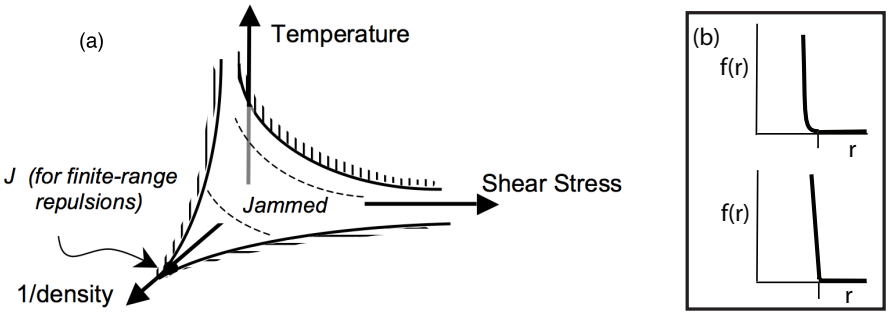

Fig. 1.1. (a) The jamming phase diagram; inside the shaded region, for high density, low temperature and small shear stress, particulate systems are *jammed*, *i.e.*, form a disordered solid phase with a finite resistance to shear. The point J is the so-called "jamming point" for spherical particles with finite-range repulsive forces. It acts like a critical point and organizes the behavior in its neighborhood. (b) The type of forces considered in models of frictionless spheres: the force $f(r)$ is of finite range, *i.e.* vanishes when the distance r between the centers of the spheres exceeds some well-defined value. The lower case, in which the force increases linearly with the compression δ, is often refered to as one-sided harmonic springs. The Hertzian force of $3d$ elastic spheres increases as $\delta^{3/2}$ and has a behavior as in the upper figure.

the ground plane of Fig. 1.1, as their relevant interaction energies are orders of magnitude larger than the thermal energy scale k_BT. While thermodynamics generally guarantees the existence of a unique phase for molecular systems at equilibrium, athermal systems strictly speaking lack the averaging needed to be able to define a unique phase: their disordered jammed states are often history dependent, a phenomenon they share with glasses.

Nevertheless, it has become clear that it is extremely useful to approach these systems with a unifying common focus in mind. For particulate systems like granular media, the constituent particles essentially have strong repulsive interactions of *finite* range: particles that are in contact do interact and repel each other, those that are not in contact, don't. A detailed analysis of the simplest model of this type, that of N repulsive frictionless spheres (or discs in two dimensions) in the large-N limit, has revealed that the point at which they just jam into a rigid phase does indeed have properties reminiscent of an asymptotic or critical point that organizes the behavior in its neighborhood. This is the jamming point, marked J in Fig. 1.1. It is the aim of this chapter to provide an introductory review of these recent findings, and to provide an outlook on the relevance of our present understanding for other systems. We aim our review of jamming on those aspects that are of most interest from the point of view of the main theme of this book, glasses. Hence we focus in particular on the various length scales that emerge near the jamming point, on the vibrational properties of the marginally jammed state above the jamming transition, and on the connection of these findings with the dynamics.

This approach bears close similarities with investigations of the rigidity of network glasses developed in the 1980's. Instead of density and shear stress, Phillips argued that the key control variable is the glass composition [2]. Based on a model of rigidity percolation proposed by Thorpe, where springs are randomly deposited on a lattice [3, 4], it was argued that glass properties are controlled by a critical point at zero temperature. The jamming transition can be viewed as a special case of the generic rigidity percolation problem in which the system self-organized to avoid large fluctuations in its structure. Thus the jamming of particles is qualitatively different from springs randomly placed on a lattice. In some respects, the jamming transition is simpler, allowing the recent conceptual progress reported here.

Unfortunately because of the focus of this book and space limitations, this chapter cannot do justice to the wonderful recent experimental developments: many new systems have become available or have been analyzed in new ways, and are increasingly driving new directions in the field of jamming. We refer for an overview of recent experiments on colloids to the chapter by Cipeletti and Weeks and for a review of experiments on grains and foams to the chapter by Dauchot, Durian and van Hecke. We will point to relevant experiments where appropriate, without going into details.

1.2 Overview of recent result on jamming of frictionless sphere packings

Close to the jamming point, packings of compressible frictionless spheres exhibit various anomalies including a strongly enhanced density of states at low frequencies. Of course, such packings are a very idealized model system for granular media. We postpone to section 1.3 a discussion of generalizations of this model such as the role of particle anisotropy and friction.

In computer models of compressible spheres, one usually uses force laws of the type sketched in Fig. 1.1(b): two spheres of radii R_i and R_j experience zero force if the distance r_{ij} between their centers is larger than $R_i + R_j$, and have a force that rapidly increases with the overlap $\delta_{ij} = R_i + R_j - r_{ij}$ if $r_{ij} < R_i + R_j$. A particularly convenient and common choice for computer models is the one-sided harmonic spring model, for which the repulsive force f_{ij} for particles in contact increases linearly with the overlap δ_{ij}. Another choice that one often encounters in the literature for compression of elastic balls, is the Hertzian force law $f_{ij} \sim \delta_{ij}^{3/2}$. In studies of three-dimensional random packings, it usually suffices to take spheres whose radii are all the same, as one easily ends up with a random packing, but in two-dimensions one needs to take a polydisperse or bi-disperse distribution of discs in order to avoid crystallization. There are various ways to prepare static packings of spheres in mechanical equilibrium. One method is to place particles randomly in a box at a fixed density and quench the system to its closest potential-energy minimum via conjugate-gradient or steepest descent algorithms [5]. Other

methods employ a slow inflation of all the radii[1] to first generate a packing at the jamming threshold where the majority of the particles experience minute forces that balance on each particle. This jamming threshold marks the onset of a nonzero pressure and potential energy. After this initial preparation the packing is compressed (or dilated) while continuously minimizing the energy [5]. Other methods slowly adjust the radii so as to steer the pressure in the packing to a prescribed value [7]. We refer to the literature for details.

We note that the onset packing fraction of the jamming transition for an ensemble of states depends on the ensemble. For systems equilibrated at infinite temperature and quenched to $T = 0$, the onset packing fraction corresponds to that of an ensemble in which each state, or local energy minimum, is weighted by the volume of its energy basin. In that case, $\phi_c \approx 0.64$ for monodisperse spheres in three dimensions [5]. However, if the ensemble is prepared by a quench from a system equilibrated at a low temperature, the onset packing fraction is higher [8, 9]. It is clear from the distribution of jamming onsets that this must be the case [5]. In the infinite-system-size limit, the distribution approaches a delta-function at $\phi \approx 0.64$ but with non-vanishing tails both on the high-density and low-density side [5]. In systems equilibrated at lower temperatures, lower energy states are weighted more heavily. Such states have higher values of ϕ_c, since the potential energy increases with $\phi - \phi_c$. Thus, the average value of ϕ_c for the ensemble must increase as the system is quenched from lower temperatures, in accordance with the results of Chaudhuri, et al. [9], and the system can be described as having a line of jamming transitions extending upwards from $\phi \approx 0.64$, as in Ref. [10]. In all cases, however, the onset pressure is zero, so the onset is sharp in terms of pressure but not packing fraction, and the vibrational properties, etc. are identical to those described below.

1.2.1 The vibrational density of states of packings

An important concept in condensed-matter systems is the density of states, $D(\omega)$. $D(\omega)\mathrm{d}\omega$ is proportional to the number of states with frequency between ω and $\omega + \mathrm{d}\omega$. Here ω refers to the frequency of the *vibrational normal modes* of the constituent particles. The density of states concept is also often used for for electronic states, but here we focus on the vibrational states of condensed matter systems. For a crystal, or in fact for any elastic medium, $D(\omega)$ increases at low-frequencies as ω^{d-1}, where d is the dimension of space. This generic behavior arises from the fact that sound modes have a dispersion relation $\omega(k)$ which is linear in the wavenumber k, together with phase-space arguments for the number of modes with wavenumber between k and $k + \mathrm{d}k$. The Debye scaling law $D(\omega) \sim \omega^2$ for $d = 3$ underlies the ubiquitous T^3 low-temperature specific heat of three-dimensional solids. It serves as an important reference

[1] This is somewhat like the Lubachevsky-Stillinger method to generate random close packings of hard spheres [6].

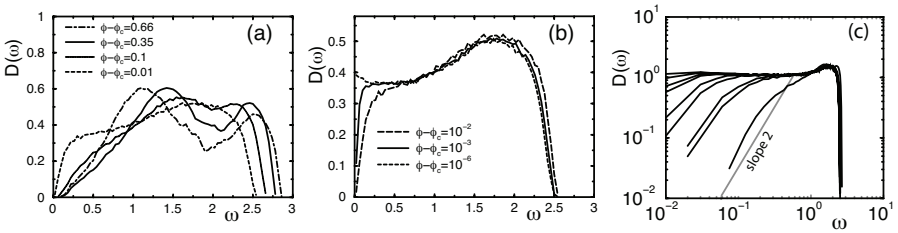

Fig. 1.2. The density of states of vibrational modes of three-dimensional soft-sphere packings with one-sided harmonic forces at varous densities: (a) significantly compressed samples; (b) close to the jamming density ϕ_c [5]; (c) on logarithmic scale [11].

for identifying anomalous behavior — *e.g.*, the well-known enhancement of the specific heat over the Debye law is an indication in glasses for an excess density of excitations at low frequencies.

To analyze the vibrational modes, one obtains the so-called dynamical matrix familiar from solid state physics. This dynamical matrix is essentially the second derivative of the inter-particle potential, and hence has only non-zero elements for particles that are in contact in the packing (for the one-sided harmonic forces these terms are especially simple as the potential is quadratic in the separation). From the diagonalization of the dynamical matrix one then obtains the eigenmodes and their eigenfrequencies ω, and hence $D(\omega)$.

Fig. 1.2 shows one of the early results for a three-dimensional packing with one-sided harmonic forces [5, 11]. Panel (a) shows that sufficiently far above jamming, $D(\omega)$ vanishes at small frequencies, in qualitative agreement with the Debye scenario, but as the density ϕ is decreased towards the jamming density ϕ_c, the weight at small frequencies increases. Indeed, closer to the jamming density $D(\omega)$ develops a plateau at small frequencies, see panel (b). When plotted on a log-log scale, as in panel (c), the crossover and the emergence of a plateau is even more clear: in these data one observes the ω^2 Debye scaling only for the largest densities, while as the packings are decompressed towards the jamming density, the plateau extends to lower and lower frequencies. Clearly, the closer the packings are to the jamming threshold, the more $D(\omega)$ is enhanced at low frequencies and the larger are the deviations from the usual Debye behavior. We will discuss in section 1.2.3 the cross-over frequency ω^*, that separates the plateau from the lower-frequency downturn.

1.2.2 Isostaticity and marginally connected solids

How do the excess low-frequency modes arise? The answer is related to the fact that at the jamming threshold, packings of frictionless discs and spheres are *isostatic*, *i.e.*, they are marginal solids that can just maintain their stability

[5, 12–17]. The origin of this is the following. Consider a disordered packing with N_c spheres or discs that have nontrivial contacts[2], with Z their average contact number. Force balance on each particle implies that the vector sum of the forces adds up to zero; therefore the requirement of force balance on all particles with contacts gives dN_c conditions. If we view the contact forces between the particles as the degrees of freedom that we have available to satisfy these requirements, then there are $ZN_c/2$ such force degrees of freedom. Clearly, assuming no special degeneracies, we arrive at the condition

$$\text{for a stable packing:} \qquad Z \geq 2d. \tag{1.1}$$

in order that force balance can be maintained.

There is a second constraint in the limit that one approaches the jamming point. As all forces are purely repulsive, in this limit almost all the individual contact forces must approach zero. For force laws like those sketched in Fig. 1.1(b), this mean that as one approaches the jamming point, all nontrivial $ZN_c/2$ contacts must obey the "just-touching" conditions $r_{ij} = R_i + R_j$. The number of degrees of freedom associated with the positions of the centers of the particles with contact is dN_c, so if we think of putting the particles with contacts in the right place to allow them to obey the just-touching conditions, we need to have

$$\text{just-touching conditions at jamming:} \qquad Z \leq 2d. \tag{1.2}$$

Clearly, the value $Z_{\rm iso} = 2d$, the isostatic value, has a special significance. Indeed, the above two conditions imply that as packings approach the jamming point, point J of Fig. 1.1(a), from the jammed side, *e.g.*, by decompressing them, one will have

$$\text{upon approaching point J:} \qquad Z \downarrow Z_{\rm iso} = 2d. \tag{1.3}$$

Note that these results are independent of the presence of polydispersity and the details of the repulsive force law, provided it is of finite range and continuous.[3]

The above argument will be further justified in section 1.2.4 for frictionless spheres. Fig. 1.3(a) shows numerical simulation results for $\Delta Z = Z - Z_{\rm iso}$,

[2] There is a subtlety here: in a typical packing there is generally a small fraction of "rattlers" or "floaters", particles in a large enough cage of other particles that, in the absence of gravity, can float freely without any contact. These should be left out from the counting below, and from the determination of the average contact numer.

[3] In passing, we note that ϕ_c, the density of a packing of monodisperse spheres (all the same radii), approaches [5] the random close packing density of hard spheres. There is an active line of research aimed at analyzing and relating the concepts of jamming and the maximally random jammed state, which has been proposed to replace the concept of the random close packed state [18, 19].

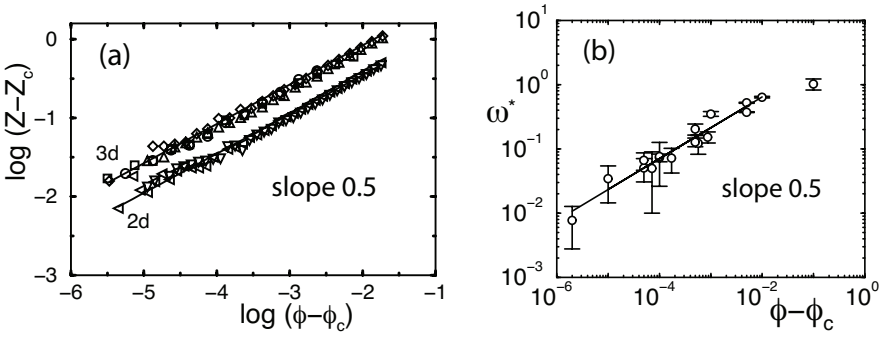

Fig. 1.3. (a) Z scales as $|\Delta\phi|^{0.5}$, from [5]. These results extend those of an earlier numerical study [20]. (b) ω^* scales as $|\Delta\phi|^{0.5}$. From [11]. Together these two sets of data are consistent with $\omega^* \sim \Delta Z$.

plotted on a log-log scale as a function of the distance from jamming, $\Delta\phi = \phi - \phi_c$, in both 2 and 3 dimensions. In both cases ΔZ goes to zero at jamming: $\Delta Z \sim \sqrt{\Delta\phi}$ [5, 20, 21]. A recent experiment aimed at testing this scaling, albeit in a system with friction, can be found in [22]. The isostaticity concept will be re-examinated in section 1.3.1 for ellipses.

Note that according to (1.1) the packings at isostaticity have just enough contacts to maintain stability. In this sense, they are marginal packings, packings at the edge of stability. Moreover, if one imagines a packing with M fewer contacts than dictated by the isostaticity condition, one can according to (1.2) deform the packing in M different directions in the space of coordinates, while respecting the just-touching constraints (so that particles are not pressed into each other). These therefore correspond to M zero-energy deformation modes in which particles slide past one another. These modes, which are in general global modes, have been called floppy modes [12, 23].

1.2.3 The plateau in the density of states and the cross-over frequency, ω^*, and length scale, ℓ^*.

The development of a plateau in the density of states is intimately connected with the approach to the isostatic jamming point. To see this, we argue as follows [24,25]. Let us start from an isostatic packing at jamming, sketched in Fig. 1.4(a). Now imagine we disregard ("cut") for a moment the bonds across a square or cube of linear size ℓ, as sketched in panel (b). There are of order ℓ^{d-1} of these surface bonds, and since the orginal packing was isostatic, by cutting the bonds at the surface we create of order ℓ^{d-1} floppy zero-energy modes within the cube. Each of these modes will be very complicated and disordered, but that does not matter here. Next, as indicated in panel (c), we use each of these floppy modes to create a variational Ansatz for a vibrational eigenmode as follows: we take each of the zero-energy floppy modes created by cutting

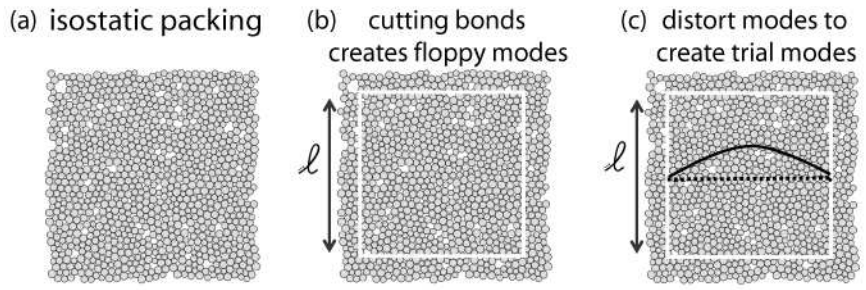

Fig. 1.4. Three stages of creating a low-energy Ansatz for a vibrational eigenmode of the system, used in the argument to derive the flatness of the $D(\omega)$ close to point J, as inspired by [24,25]. In (c), the solid line illustrates the behavior of the smooth amplitude with which the underlying floppy mode is distorted, and which vanishes at the boundaries of the box. See text for details.

bonds, and distort it by a smoothly-varying sine-like amplitude which vanishes at the boundaries of the box, right at the point where we have artifically cut the bonds. This long-wavelength distorted mode is a good Ansatz for a low-energy eigenmode: when we analyze the potential energy associated with this Ansatz-mode, the underlying floppy mode does not contribute to the energy — only the fact that the mode has been made imperfect by the elastic distortion on the scale ℓ contributes at every bond a distortion energy of order $1/\ell^2$ (nearby displacements differ from that in the underlying floppy modes by an amount of order the gradient of the amplitude, so the energy, which involves terms of order the average compression squared, is of order $1/\ell^2$). Hence this Ansatz mode will have a frequency $\omega_\ell = \mathcal{O}(1/\ell)$.

Of course, in a variational calculation, each of these Ansatz modes will acquire a lower energy upon relaxation, but the number of them will not change (rigorously speaking this argument yields a lower bound on the density of states). In what follows we shall call the modes obtained from the distortion of floppy modes 'anomalous', as their nature is very different from that of plane waves. Assuming that the energy does not shift dramatically, we have created $N_\ell \simeq \ell^{d-1}$ modes with frequency up to $\omega_\ell \sim \ell^{-1}$ in a box with of order $V_\ell \sim \ell^d$ particles. Thus we have

$$\int_0^{\omega_\ell} \mathrm{d}\omega D(\omega) \simeq \frac{N_\ell}{V_\ell} \sim \frac{1}{\ell}. \tag{1.4}$$

If we assume that $D(\omega)$ scales as ω^q for small frequencies, we get

$$(\omega_\ell)^{q+1} \sim \frac{1}{\ell^{a+1}} \sim \frac{1}{\ell}, \tag{1.5}$$

which immediately yields $a = 0$: $D(\omega)$ is flat at low frequencies.

When the packings are compressed so that they have an excess number of bonds $\Delta Z = Z - Z_c$, the above line of reasoning can also be followed to

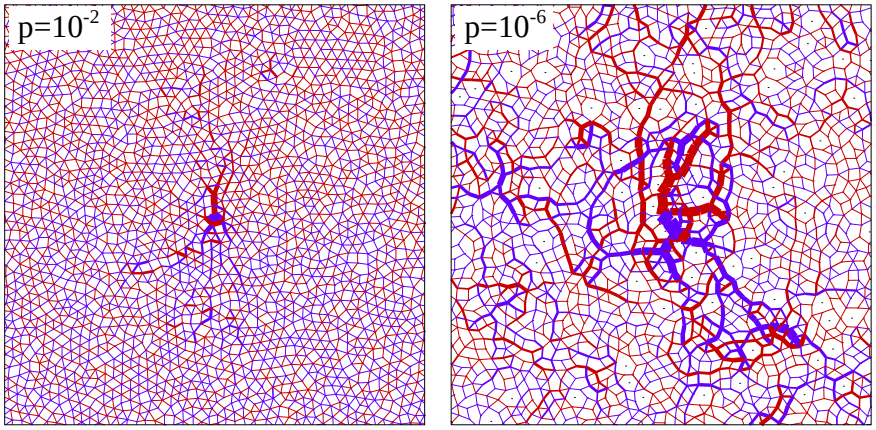

Fig. 1.5. Illustration of the fact that the length scale ℓ^* increases as the jamming threshold is approached. This figure illustrates the response to a force loading in the center, with blue (red) lines indicating an increase (decrease) of the force at a contact; the thickness of the lines is proportional to the size of the change in force. The left panel is for a pressure $p = 10^{-2}$, the right one is close to the jamming point, *i.e.*, at pressure $p = 10^{-6}$. In the latter case, the fluctuations are larger and extend over a larger region. A detailed analysis shows that this range grows proportionally to the length scale ℓ^*. From Ellenbroek *et al.* [26, 27].

obtain the cross-over frequency ω^* and length scale ℓ^* that separate the range dominated by isostaticity effects from the usual elastic behavior. Instead of starting from an isostatic packing, we retrace the above construction for a packing with given excess contact number ΔZ per particle. The total number of excess bonds within the box of Fig. 1.4(b) then scales like $\Delta Z\, \ell^d$. If the number of degrees of freedom $N_\ell \simeq \ell^{d-1}$ created by cutting bonds at the boundary of the box is less than the excess number of bonds in the bulk, no zero-energy modes will be created. This fact was already noticed by Tkachenko and collaborators in inspiring works [14,15]. Hence we expect a cross-over scale ℓ^* when the two terms balance,*i.e.*, when

$$N_{\ell^*} \simeq (\ell^*)^{d-1} \simeq \Delta Z\, (\ell^*)^d \quad \Longrightarrow \quad \ell^* \sim 1/\Delta Z. \tag{1.6}$$

Likewise, according to the argument above, one expects the crossover frequency ω^* in the density of states above jamming will scale as

$$\omega^* \sim 1/\ell^* \sim \Delta Z. \tag{1.7}$$

The scaling of the cross-over frequency, $\omega^* \sim \Delta Z$, has been well documented from a detailed analysis of the density of states, as shown in Fig. 1.2. At finite compression, ω^* is the frequency above which there is a plateau in $D(\omega)$, and below which $D(\omega)$ decreases with decreasing frequency. Early data obtained as a function of excess density $\Delta\phi$ are shown in Fig. 1.3(b), and are

found to scale as $\omega^* \sim |\Delta\phi|^{0.5}$. Since $\Delta Z \sim |\Delta\phi|^{0.5}$, see Fig. 1.3(a), this is consistent with the scaling $\omega^* \sim \Delta Z$. An explicit plot of ω^* versus ΔZ can be found in [24].

We stress that in the above argument, it is implicity assumed that the bond strength k remains unchanged. This is true for one-sided harmonic forces, but not for Hertzian interactions which weaken upon approaching the jamming point: $f \sim \delta^{3/2}$ so that $k \sim \delta^{1/2} \sim \sqrt{\Delta\phi}$. Since frequencies scale as $\sqrt{k}$, the above arguments generalize to non-harmonic forces if formulated in terms of scaled frequencies $\tilde{\omega} = \omega/\sqrt{k}$.

While the cross-over frequency is relatively easy to extract from the vibrational density of states, the cross-over length ℓ^* is more difficult to extract from a mode or from response data. Physically, ℓ^* is the length scale on which the lowest-frequency anomalous modes probe the microscopic structure of the solid, and are therefore sensitive to its fluctuations. Thus one may expect to observe ℓ^* in the fluctuations of the linear response of the solid, rather than in its mean behavior. Another difficulty lies in the fact that the floppy modes which form the basis for the behavior up to scale ℓ^* are very disordered so that a weak, elastic-like distortion of such modes is difficult to detect. Nevertheless, it has been discovered that the cross-over length is easily discernable by eye in the response to a point force or to inflation of a local particle [26,27], as Fig. 1.5 illustrates. A detailed analysis of these data has indeed shown that the response is governed by a crossover scale that grows as $1/\Delta Z$, in accord with (1.6).

1.2.4 Microscopic criterion for stability under compression

So far our analysis of the density of states has neglected the effect of pressure on the vibrational spectrum. Mundane observations such as the buckling of a straw pushed at its tips show that compression affects vibrational modes, and can even make them unstable. In general, this effect is important for thin objects, but is irrelevant at small strain for bulk solids where plane waves dominate the vibrational spectrum. However compression plays an important role if floppy modes are present in the solid, as noticed by Alexander in the context of gels [12]. As we now show, this is also true for the anomalous modes introduced above [25].

The analysis is based on the well-known observation, see Fig.(1.6), that if k is the stiffness associated with the longitudinal relative displacements of two particles in contact, then for transverse displacements the stiffness is $k_1 \propto -ke$, where e is the contact strain. For a pure plane wave propagating in an amorphous solid, the transverse and longitudinal components of the relative displacements in the contacts are of the same order. The correction induced on the mode energy by the presence of a finite contact force or strain is thus, in relative terms, of order of the ratio of the two stiffnesses: $-e$. Therefore the effect of compression on plane waves is negligible at small strain. For anomalous modes the situation is different, because they are built

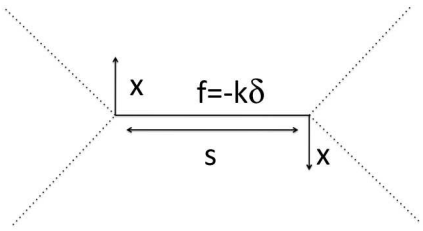

Fig. 1.6. Consider for concreteness a harmonic contact between two particles of length s, of stiffness k, carrying a force $f = -k\delta$ where δ is the contact elongation. If particles moves transversally to the contact by an amplitude x as shown with vertical arrows, the contact length increases by an amount proportional to x^2/s following Pythagorus theorem. The work produced by the contact force is then proportional to $x^2 k\delta/s$, corresponding to a stiffness $k_1 \sim k\delta/s \equiv -ke$, where $e \equiv -\delta/s$ is the contact strain, chosen to be positive for compressed contacts.

by deforming floppy modes that have no longitudinal relative displacements, but only transverse ones. Once floppy modes are deformed to generate anomalous modes, they gain a longitudinal component of order ΔZ as follows from the variational argument, whereas the transverse component remains of order one [17, 25]. Relative corrections in the anomalous mode energies is thus of order $-e/\Delta Z^2$. When these relative corrections reach a constant of order one, anomalous modes become unstable, and the system yields. For particles near jamming, one has $e \propto \Delta\phi$, leading to the condition for stability [25]:

$$\Delta Z > \Delta\phi^{1/2} \qquad \text{for all subsystem of size } L > l^* \tag{1.8}$$

where a numerical pre-factor is omitted. Inequality(1.8) extends Maxwell criterion to the case of finite compression and is also not a local criterion: it must be satisfied on all subsystems of size larger than l^*. On smaller scales, fluctuations of coordination violating Eq.(1.8) are permitted, as stability can be insured by the boundaries. Configurations where the bound (1.8) is saturated are marginally stable and anomalous modes exist down to zero frequency. Such packings should exhibit the scaling $\Delta Z \sim \Delta\phi^{1/2}$. Configurations obtained by decompression in the vicinity of ϕ_c appear to lie very close to saturation [25]. The scaling of Eq.(1.8) was proposed independently by Head [28] following a mean-field analysis; there, however, the threshold coordination found was half its correct value.

An argument for why one might expect the system to be marginally stable is provided in section 1.6.1, where it will be argued that the realization of the bound (1.8) critically affects the dynamics. The criterion (1.8) applies to spheres, but not to ellipses where rotational degrees of freedom matter. It can be shown that in the later case, compression can have a *stabilizing* effect

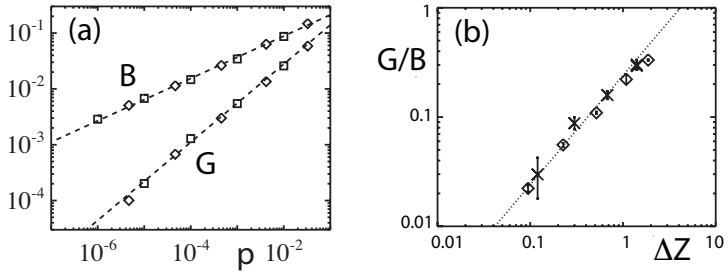

Fig. 1.7. (a) As the jamming point is approached, in this case by lowering the pressure, the shear modulus G becomes much smaller than the bulk compression modulus B [5, 20]. These results are for packings with Hertzian forces, for which the bond strength of individual forces scales as $p^{1/3}$. Due to this weakening of the bonds, the bulk modulus B has an overall $p^{1/3}$ scaling, while the shear modulus G has an overall $p^{2/3}$ scaling. (b) The ratio G/B is linear in Δz [5, 20]; this scaling is independent of the force law. Squares refer to data obtained from response to a local point force, diamonds to data obtained from a global deformation. After [26, 27].

if the ellipses make in average more contacts where their surface curvature is low. In that case, even an infinitesimal pressure can stabilize zero-modes, so that stable packings can be generated although the Maxwell bound is not fulfilled, as shown in section 1.3.1. The same is true for gels of cross-linked polymers [12].

1.2.5 Behavior or elastic constants near jamming

The fact that a packing of frictionless spheres or discs is a marginally-connected solid, also has its effect on the elastic constants. The behavior of the bulk compression modulus B and shear modulus G always depends on the specific force law, and hence is not universal: for distributions of bonds which are peaked around some average non-zero value, both of them are proportional to the average bond strength k, hence in discussing the effects due to jamming it is useful to divide out this common effect. The individual bond strength k_{ij} are essentially the second derivatives of the interaction potential evaluated at each contact — for the one-sided harmonic springs these are all the same, but for the Hertzian $f_{ij} \sim \delta_{ij}^{3/2}$ force law one finds $k_{ij} \sim \delta_{ij}^{1/2} \sim f_{ij}^{1/3}$, so that the average bond strength scales with the pressure p as $p^{1/3}$.

An example of data for the elastic moduli is shown in Fig. 1.7, which summarizes data for B and G for packings of two-dimensional discs interacting with Hertzian forces [26, 27]. The bulk modulus B is clearly seen to scale as $p^{1/3}$ [5], which as we argued above is the scaling of the average bond strength for this force law. However, G decreases much faster, as $p^{2/3}$ [5]: packings close to jamming are much easier to distort by shear than by compression. Results in both two and three dimensions for harmonic [5, 20] and Hertzian

potentials [5] have been determined. From these results, it is generally seen that G/B and ΔZ scale in the same way with compression. The data in Fig. 1.7 are consistent with this, as for a Hertzian interaction, $G/B \sim p^{1/3}$ and $\Delta Z \sim |\Delta\phi|^{0.5} \sim p^{1/3}$. The result that the shear modulus generally scales as $G \sim k\,\Delta Z$, can be understood [17]: independent of the force law, the ratio G/B should scale as $G/B \sim \Delta Z$. Empirical support for this behavior in grains is reviewed in [29].

It is interesting to note that at first sight the fact that G/B goes to zero at the jamming point as ΔZ, may seem to be the anomalous behavior; however, from the point of view of rigidity percolation [30], B/k behaves anomalously for packings, as in rigidity percolation both G/k and B/k vanish as ΔZ, upon approaching the isostatic point so that G/B remains constant at the percolation threshold. The difference between the jamming transition and generic rigidity percolation is that in the former case configurations must be such that all the contact forces must be repulsive. This imposes a geometric constraint on the network that is not enforced in standard rigidity percolation models [17]. We refer to [31] for further details.

To compute static properties such as G/B theoretically, one may use effective medium theory. This approach has been used to study a square lattice with randomly placed next-nearest-neighbor springs [32] and random isotropic off-lattice spring networks [33,34]. In the isotropic case (rigidity percolation), G/B is independent of ΔZ at the transition, as found in Ref. [31], while in the randomly decorated square lattice $G/B \sim \Delta Z^2$. Both results differ from the scaling observed for jammed packings, $G/B \sim \Delta Z$.

An important topic in granular research has been the issue of the coarse graining scale needed for elastic behavior to emerge in granular packings [35, 36]. In line with the arguments given above, it has been found that near the jamming point, one needs to coarse grain over the scale ℓ^* to see elastic response emerge [26, 27]: as one approaches the jamming point, one has to coarse grain over larger and larger lengths, diverging as $\ell^* \sim 1/\Delta Z$. That elasticity emerges in granular media on long enough scales is also implicitly confirmed by the data of Fig. 1.7, where squares give the values of the elastic constants obtained from local point response calculations, and diamonds those obtained from global deformations. The two sets of data agree very well [26, 27].

1.2.6 Diffusivity, quasilocalized modes and anharmonicity

Diffusivity

The excess low-frequency vibrational modes associated with the isostatic jamming transition have important consequences for the nature of energy transport in the system. Their contribution to energy transport can be quantified by the energy diffusivity, defined as follows [37, 38]. Consider a wavepacket narrowly peaked at frequency ω and localized at $\boldsymbol{r}$. This wavepacket spreads

out in time, such that the square of the width of the wavepacket at time t, divided by t, is independent of t at large t; this constant defines the diffusivity, $d(\omega)$. The diffusivity was calculated using the Kubo approach within the harmonic approximation for repulsive sphere packings as a function of compression in [39, 40]. At sufficiently low frequencies, the modes should be plane-waves and the diffusivity should follow Rayleigh scattering behavior so that $d(\omega) \sim \omega^{-4}$. Refs. [39, 40] show that the diffusivity is nearly flat for frequencies from ω^* up to the Debye frequency, where it drops to zero. Thus, there is a crossover from weakly-scattered plane waves to strong-scattering, diffusive behavior at ω^*; this can be understood from the heterogeneous nature of the anomalous modes [17, 40], or by assuming the continuity of the length scale characterizing plane waves and anomalous modes at the crossover frequency, in conjunction with the scaling laws for the shear and bulk moduli discussed in section 1.2.5 [39, 40].

One consequence of the link between the transport crossover and the excess modes [39, 40] is that the diffusivity plateau extends all the way down to the lowest frequencies studied as the jamming transition is approached and $\omega^* \to 0$, as shown in Fig. 1.8(a). This suggests that the origin of the diffusivity plateau can be traced to properties of the jamming transition.

Dynamical vibrational properties such as the energy diffusivity can be computed theoretically using dynamical effective medium theory, a re-summation scheme of a perturbation expansion in the disorder also known as the Coherent Potential Approximation (CPA) [41]. This approach has been used on the square lattice with randomly placed next-nearest-neighbor springs [32] and isotropic disordered spring networks near the isostatic limit [34]. Both calculations yield a crossover to a flat density of states above $\omega^\star \sim \Delta Z$ in good agreement with results for jammed packings. In the isotropic case, Rayleigh scattering is found for $\omega < \omega^\star$ with a scattering length $\ell_s \sim \Delta Z^3/\omega^4$. This calculation predicts a violation of the Ioffe-Regel criterion (according to which the cross-over to strong scattering occurs when the scattering length becomes of order of the wavelength) at the crossover frequency $\omega^\star$ since the scattering length $\ell_s \sim 1/\Delta Z$ is much larger than the wavelength $\lambda \sim 1/\sqrt{\Delta Z}$ there. Above $\omega^\star$, the anomalous modes are characterized by a displacement-displacement correlation length that scales as $1/\sqrt{\omega}$, which scales as $1/\sqrt{\Delta z}$ at $\omega^\star$, and a frequency-dependent speed of sound, $c(\omega) \sim \sqrt{\omega}$. This leads to a plateau in the diffusivity consistent with the results of Fig.(1.8). This analysis predicts a drop in the speed of sound near ω^*, a subtle effect recently observed numerically at the Boson peak frequency in model glasses [42]. In the case where the isostatic state is a square lattice [32], the Ioffe-Regel criterion is satisfied at the crossover frequency ω^* and ℓ_s is of order the lattice spacing. Numerical results for jammed packings are consistent with $\ell_s \sim 1/\sqrt{\Delta z}$ at the crossover.

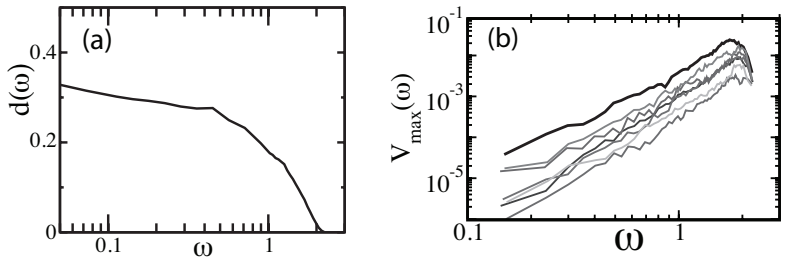

Fig. 1.8. (a) Diffusivity, $d(\omega)$, for a system of spheres interacting via harmonic repulsions very close to the jamming transition. $d(\omega)$ is essentially flat down to zero frequency. From Xu *et al.* [43]. (b) Energy barrier $V_{\max}(\omega)$ along each mode, before falling into another basin of attraction for a system at $\Delta\phi = 0.1$. The energy barriers along each mode direction provide an upper bound on the energy barriers of the system in a given frequency range, since it is possible that lower energy barriers could be encountered in directions in phase space corresponding to linear combinations of the modes. From [44].

Quasilocalized modes

The nature of the excess low frequency modes shows a systematic variation with frequency. As the frequency is lowered towards ω^*, numerical studies of three-dimensional sphere packings show that the modes become progressively more heterogeneous with a lower-than-average mode coordination number, and develop high displacement amplitudes in small regions of space [39]. These quasi-localized modes shift downwards with decreasing compression. These low-frequency, quasi-localized modes have also been observed in two-dimensional packings of soft disks [45], but here the quasi-localized modes are mixed in with plane-wave-like modes over the same low-frequency range.

In three dimensions, the frequency of the quasi-localized modes decreases with compression, but the degree of quasi-localization does not appear to depend on compression. This suggests that as the system is decompressed towards the unjamming transition, quasi-localized modes always exist but shift to lower and lower frequency. Quasi-localized modes have been observed in other disordered models [46–49] and in experiments on glassy polymers [50–52]. In the soft-potential model, for example, such modes have been shown to lead to strong scattering of vibrations at higher frequencies, so that their frequency corresponds to the Ioffe-Regel crossover frequency in the transport properties [53], while in model silica, these modes have been identified near the boson peak frequency [48].

Numerical studies on hard spheres [54,55] have shown that irreversible particle rearrangements at nonzero temperature occur along the low-frequency modes, observed to be extended in the systems of limited size studied, implying that the lowest activation barriers are in those directions of phase space (Sec. 1.6.1). This view has been explored in model glasses [56], which

have also shown that the structural rearrangements occurring at finite temperatures were along low-frequency normal modes, which in that case were quasi-localized.

Fig. 1.8(b) shows that for sphere packings, the low-frequency quasi-localized modes have the lowest energy barriers and that the energy barriers decreases systematically with frequency and participation ratio. This result, together with previous observations [54–56], should have important consequences for the dynamics and instabilities that occur as the temperature is raised from zero, the system is compressed, or a shear stress is applied. One would expect these modes to shift downwards to zero frequency under the last two circumstances [57] and to give rise to highly heterogeneous deformations in the sample. These could be the underlying mechanism for the localized deformations postulated in the picture of shear transformation zones [58, 59].

As the system is decompressed towards the unjamming transition, the barriers between nearby configurations shrink to zero as the amount of interparticle overlap decreases to zero. Thus, in this limit the modes become progressively more anharmonic. This implies that smaller excitation energies or temperatures should suffice to force the system into new energy minima. Thus, the range of temperatures and stresses over which harmonic theory applies should shrink to zero and anharmonic effects should dominate as one approaches the transition. This effect has been computed in networks of springs below or above the isostatic threshold [60], where non-linearities dominate the response to shear when the strain γ is larger than some γ^*, with $\gamma^* \sim |\Delta z|$.

1.2.7 Structural features of the jamming transition

At point J, the pair distribution function has many singular properties [5, 61]. In particular, it has been shown that the first peak in $g(r)$ is a δ-function at the nearest neighbor distance, σ. The area under this δ-function is just the isostatic coordination number: $Z = 6$ in three dimensions. On the high side of this δ-function, $g(r)$ has a power-law decay: $g(r) \propto (r - \sigma)^{-0.5}$. It has been proposed that this power-law is the vestige of the marginal stability of the configurations visited before reaching ϕ_c [17]. Also, at the jamming transition, the second peak of $g(r)$ is split into what appear to be two singular sub-peaks one at $r = \sqrt{3}\sigma$ and the other at $r = 2\sigma$. There is a divergent slope just below each subpeak and a step-function cutoff on its high side [61].

The pair correlation function near the zero-temperature jamming transition has been studied in two experiments. In experiments by Abate and Durian [62,63], a layer of ball bearings were placed on a wire mesh and excited by the upflow of gas through the mesh. The turbulent flow of the gas leads to interactions between the balls and to random motion of the balls. Thus, the effective interaction potential between the balls can be characterized by a hard core determined by the ball diameter and a longer-ranged repulsion due to the gas. In such systems, the kinetic energy of the balls decreases monotonically with increasing density of the balls, such that it reaches zero when the balls

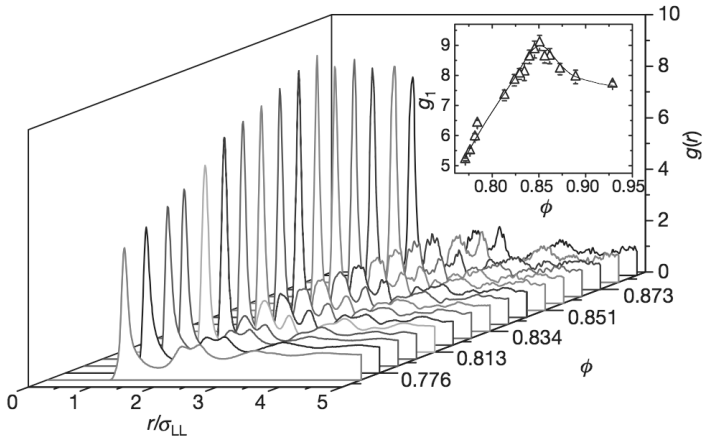

Fig. 1.9. Pair-correlation function $g(r)$ for the large particles at different packing fractions ϕ for a bidisperse system of colloids in two dimensions. The inset shows g_1, the height of the first peak of $g(r)$, versus packing fraction. The experimental data shows that g_1 is non-monotonic with a maximum at a packing fraction slightly above ϕ_c, the value at the $T = 0$ jamming transition. The peak is a vestige of that $T = 0$ transition where the first peak of $g(r)$ is a δ-function. Figure reproduced from [65].

are packed to the density of the jamming transition, $\phi_c \simeq 0.84$, measured in terms of the hard-core diameter. The structure of the system, as characterized by the pair correlation function, $g(r)$, was studied along this trajectory to the zero-temperature jamming transition of the hard cores (See the chapter in this book by Dauchot, Durian and van Hecke for a description of the dynamical properties of this system). On approaching ϕ_c, the structure shows an increase of the height of the first peak, g_1. This is consistent with numerical results on soft spheres, which find a divergence in g_1 at the zero-temperature jamming transition. There is also a local maximum in g_1 at $\phi \approx 0.74$, above which no changes in the coordination and geometrical features of Voronoi cells are observed. This secondary maximum at nonzero kinetic energy due to airflow-induced interactions, may correspond to the finite-temperature vestige [64] of the divergence in the height of the first peak of $g(r)$ at the zero-temperature transition discussed below.

Experiments on a two-dimensional bidisperse system of NIPA particles by Zhang, et al. [64], measured the pair correlation function as a function of density at essentially fixed, nonzero temperature. The system exhibits a maximum in the height of the first peak of the pair correlation, g_1 — see Fig. 1.9. This maximum is interpreted as a thermal vestige of the zero-temperature jamming transition. Corroborating simulations show [64] that the divergence in $g_1 \sim 1/(\phi - \phi_c)$ for soft repulsive spheres at the zero-temperature jamming transition is softened to a maximum at nonzero temperature. The maximum

in g_1 decreases in height and shifts to higher density with increasing temperature. The simulations also show that the maximum in g_1 is a structural feature that is apparent as a function of increasing density at fixed temperature, but not as a function of temperature at fixed density or pressure. Recent simulations on the same model by Jacquin, et al. [66] show that the maximum in g_1 appears even in systems at higher temperature or lower pressure that are in thermal equilibrium and can be understood from liquid state theory.

Note that the divergence in g_1 corresponds to a vanishing of the overlap distance between neighboring particles. Thus, tracking g_1 is equivalent to tracking the overlap distance. The evolution of the overlap distance with temperature is not correlated with the existence of a dynamical glass transition.

1.2.8 Singular length scales at Point J

Several different singular length scales have been identified near the jamming transition. The cutting length, ℓ^*, discussed in Sec. 1.2.3, has been observed by studying the fluctuations in the change of the force on a contact as a function of the distance of the contact from a small local perturbation (see Fig. 1.5). This length scale diverges as $(\phi - \phi_c)^{-1/2}$, independent of the potential as long as it is repulsive and finite in range. In addition, this length scale is expected to correspond to the wavelength of longitudinal, weakly-scattered plane waves just below the crossover frequency ω^* [11], although it has not been seen numerically, due to the small system sizes that can be studied.

A second diverging length scale has been identified from the wavelength of transverse, weakly-scattered plane-waves just below the crossover frequency ω^* [11,40]. This length scale diverges as $(\phi-\phi_c)^{-1/4}$. Finally, this length scale emerges within the effective medium approximation as the decay length for spatial correlations in modes at the frequency $\omega \to \omega^\star+$ [34].

As noted in Sec. 1.2.5, there is a vanishing length scale corresponding to the overlap distance δ between neighboring particles. This distance, which measures the lefthand width of the first peak of the pair-correlation function, vanishes as $(\phi - \phi_c)^1$ [5, 67].

Finally, there are other diverging length scales whose origins are not understood. The shift of the position of the jamming transition, ϕ_c, with the linear size of the system, L, yields a length scale that apparently diverges as $|\phi-\phi_c|^{-0.7}$ in both 2 and 3 dimensions [5]. This scaling shows up in simulations in which a hard disk is pushed through a packing below ϕ_c; the transverse distance over which the packing adjusts as the disk passes by diverges with a power-law of 0.7 [68]. Finally, this power-law has been observed for correlations of the transverse velocity on athermal, slowly-sheared sphere packings near the jamming transition [69]. However, this length scale is only observed for certain models of the dynamics [70].

1.3 Extensions of the results for frictionless spheres

1.3.1 Anisotropic particles: ellipsoids

The counting of degrees of freedom that underlies the above analysis of the soft modes near the jamming point, relies on having perfect spherical and frictionless particles. We briefly review here what happens to the jamming scenario if the particles are frictionless but non-spherical.

The model for which this question has been studied in detail is that of two-dimensional frictionless ellipses in two dimensions [71] or ellipsoids with one axis of symmetry in three dimensions [45]. In the latter case, each ellipsoid is essentially characterized by 5 nontrivial degrees of freedom, so a naive counting of the degrees of freedom shows that the isotropic values for such ellipsoids is $Z_{\rm iso}^{\rm ellipsoid} = 2 \cdot 5 = 10$.

Clearly, while the isotropic values jumps depending on which degrees of freedom are, and which ones are not, included in the counting, one would expect the physical behavior of such packings to evolve continuously, when the a-sphericity of the particles is turned on — what is happening?

Let us take the c axis of our ellipsoids along their symmetry axis; the other axes are then a and $b = a$. We define the ellipticity as the aspect ratio $\varepsilon = c/a$, so prolate ellipsoids (like cigars) correspond to $\varepsilon > 1$ while oblate ones (like M&M's [72]) to $\varepsilon < 1$. Fig. 1.10(b) recovers the finding of [72–75] that as the ellipticity is tuned away from the spherical case $\varepsilon = 1$, the average contact number indeed increases continuously from the spherical value $Z_{\rm iso} = 6$, as expected.

How to resolve this apparent paradox between the jump in the counting and the continuity of the physical system? How come one can reach values of the average contact number below the isostatic value $Z_{\rm iso}^{\rm ellipsoid} = 10$? To answer these questions, it is good to realize that when we reached the conclusion that the isostatic value $Z_{\rm iso}^{\rm sphere} = 2d = 6$, we left out the rotational degrees of freedom of each sphere, as these are trivial zero-frequency modes (three per particle) for a system of frictionless spheres. In order to understand the continuity, it is better to include these rotational degrees of freedom from the start, even for the spherical case, and see how they evolve when the spheres are deformed into ellipsoids. Since in the work [45] that we will summarize below, the ellipsoids still have one symmetry axis, there are only two nontrivial angular degrees of freedom associated with the anisotropy of these particles. The relevant isostatic value for these ellipsoids of revolutation is therefore $Z_{\rm iso}^{\rm ellipsoid} = 2 \cdot 5 = 10$, as already asserted above.

When analyzed more carefully, the counting arguments summarized in section 1.2.2 imply that whenever $Z < Z_{\rm iso}$, there are $N_c(Z_{\rm iso} - Z)/2$ directions in the phase space of the relevant coordinates of the particles along which the packing coordinates can be changed without changing the interaction energy of the particles. This means that each stable configuration must have precisely this number of zero-frequency modes. That this is precisely what happens in

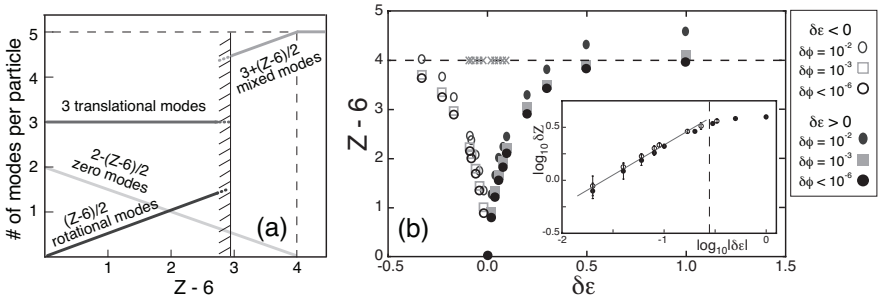

Fig. 1.10. (a) Illustration of how the number of different modes per ellipsoid (excluding rattlers) in the packings at jamming varies as a function of the average contact number Z. As the ellipticity is increased, the average contact number increases. For $Z <\approx 9$, there are two well-defined bands: a rotational band with $(Z-6)/2$ modes per particle and a translational band with three modes per interacting particle as is the case for spheres (see Fig. 1.11 for details). Upon increasing Z, the number of zero modes decreases as zero-modes are converted into finite-frequency rotational modes. Above $Z \approx 9$, there is only one band. (b) Z as a function of the ellipticity $\delta\varepsilon \equiv \varepsilon - 1$ and distance from jamming $\delta\phi$ for 216-particle packings. The sharp decrease around the spherical case $\delta\varepsilon = 0$ is consistent with earlier results [72, 74, 75] for hard ellipsoids and spherically capped rods. The log-log plot of δZ versus $|\delta\varepsilon|$ in the inset shows that the rise of Z at jamming is consistent with a $\delta Z \sim \sqrt{|\delta\varepsilon|}$ scaling. The crosses in the main plot for small values of $\delta\varepsilon$ show that twice the measured number of zero-frequency eigenmodes per particle plus $Z-6$ add up precisely to 4, in accord with panel (a). From Zeravcic *et al.* [76].

the ellipsoid packings, is illustrated by the grey crosses in Fig. 1.10(b); numerically it is found that in the calculation of the density of states of ellipsoid packings one finds precisely the right number of zero modes as expected according to this argument.

Fig. 1.10(a) illustrates how, as Z increases with $\delta\varepsilon = \varepsilon - 1$ of the ellipsoids, the number of zero modes per particle with contacts goes down. We thus have more and more nonzero modes as Z increases. What is their nature? Fig. 1.10(a) shows that for $|\delta\varepsilon| < 0.17$, the density of states exhibits two clearly separated bands [45]. The modes in the upper band of the density of states turn out to be predominantly translational — they are very similar to those found in the sperical packings, and turn out to be characterized by an onset frequency ω^* that scales as $\Delta Z = Z - 6 \sim |\delta\varepsilon|^{1/2}$: even though contacts at jamming are created by deforming the particles and not by compression, the mechanism that determines the onset of anomalous translational modes at a frequency ω^* is the same! Furthermore, the lower frequency band that exisits for small ellipticity consists of predominantly rotational modes; it is characterized by an upper frequency that scales linearly in $|\delta\varepsilon|$ [45]. For excentricities larger than about 0.17, the two bands merge into one mixed band, as Fig. 1.10(b) illustrates.

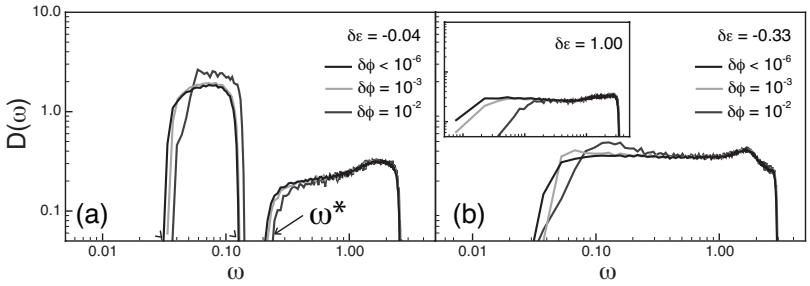

Fig. 1.11. (a) The density of states for slightly oblate ellipsoids, $\delta\varepsilon = -0.04$, for packings close to jamming and at two compressions. The existence of two bands separated by a gap as well as a gap at zero frequency is clearly visible. (b) For larger ellipticities the two bands merge, as is illustrated here for $\delta\varepsilon = -0.33$. The inset shows the data for $\delta\varepsilon = 1$ where $Z \approx Z_c = 10$ at jamming (see panel a). In accord with this, the gap near zero frequency increases with increasing compression (and therefore increasing Z). From Zeravcic *et al.* [76].

The scenario that emerges for the number of modes in the various bands is summarized in Fig. 1.11(a) — the upshot is that the jamming scenario as formulated for frictionless spheres, as exemplified by the sharp onset of anomalous modes, withstands the change in shape of the particles in the system.

1.3.2 Packings of frictional spheres

Another relevant extension is to include static friction in the force law. The usual friction law is to take the Mohr-Coulomb law [77], in which the particles can experience a tangential force f_t which obeys $f_t \leq \mu f_n$, where f_n is the normal force at the contact considered, and μ the Coulomb constant. In the Hertz force-law model, the tangential elastic force builds up continuously, in a well-described way, when a contact gets loaded with a tangential force [77]. This buildup continues up to μf_n, beyond that f_t remains constant and fixed at the value μf_n. In the presence of static friction, therefore, the properties of a packing are very history dependent, as the tangential forces are not only dependent on the configuration, but also on how the configuration was made — see e.g. [78–81].

If we return to spherical particles, but include the Mohr-Coulomb friction law, again the counting of the number of degrees of freedom is different: the coordinates of the centers of the particles are still the degrees of freedom with which one can satisfy the "just touching conditions" (1.2) upon approaching the jamming point. On the other hand, the counting of the degrees of freedom in the force and torque balance conditions is different — e.g., in two dimensions the frictional forces add one additional tangential frictional force component for each contact, but torque balance only adds one extra constraint per particle. A straightforward generalization (see e.g. [7]) shows that

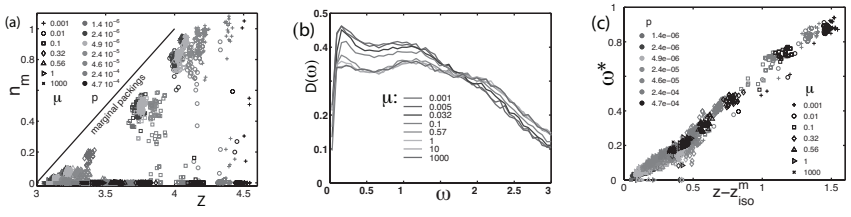

Fig. 1.12. Data from Henkes *et al.* [83] on frictional packings. (a) In gently prepared frictional packings, there a finite fraction of the contacts is found to lie at the mobilization threshold (are "fully mobilized"), i.e., has $f_t = \mu f_n$. In this diagram a large number of packing configurations are plotted in a diagram of Z and n_m, the average number of fully mobilized contacts per particle. For lower pressure, the dots in this diagram representing the packings approach the generalized isostaticity line, defined by (1.9), where packings are marginal. (b) Density of states for the lowest pressure data for a large range of values of the friction μ. In all cases the density of states is strongly enhanced at low frequencies. The frequency plotted here is actually the scaled frequency $\tilde{\omega}$ mentioned in section 1.2.3. (c) The cross-over frequency ω^* scales as $\Delta Z = Z - Z^m_{\rm iso}$.

in general with frictional forces stable packings can be obtained provided that $d+1 \leq Z \leq 2d$. Unlike for the frictionless case, where this argument dictates Z completely in the limit that the jamming point is approached, the inclusion of a static frictional force allows a range of possible values of Z. In simulations of frictional systems, it is indeed indeed found that packings at the jamming threshold with different values of Z and density ϕ can be made, by varying in particular the quench rate; moreover, there is a clear trend for the average contact number Z to approach the lower lower limit $d+1$ — the isostatic value in the presence of friction — in the limit $\mu \to \infty$ [7, 82]. In line with this, one finds that if one studies the linear vibration-rotation modes of these packings, the density of states only develops a plateau in this large friction limit [81].

However, it was later discovered that the situation is more subtle. If packings are prepared gently, then one finds that a finite fraction of the contacts in the simulations are at the mobility or Coulomb threshold, *i.e.*, have $f_t = \mu f_n$ [7, 83]. If such a contact is pushed in the direction of increasing friction force, they slip! In other words, a finite fraction of the tangential forces is *not* arbitrary, but constrained to be at the Coulomb threshold. This of course changes the counting of the number of degrees of freedom. Indeed, if one introduces n_m, the number of contacts per particle which is found at the mobility threshold, then one may introduce a generalized criterion [7, 83]

$$Z \geq (d+1) + \frac{2n_m}{d} \equiv Z^m_{\rm iso}. \tag{1.9}$$

for the stability of packings. In this scenario, packings which are close to the line $Z = Z^m_{\rm iso} = d+1+2n_m/d$ are again marginal, *i.e.*, develop many low-lying

excitations because the number of contacts that slip under tangential motion is just large enough to make almost zero-energy deformations possible. The idea that gently prepared packings might end up being marginal packings in this way, traces back to an earlier suggestion by Bouchaud [84].

With this generalization, packings with static friction that are gently prepared, do again follow in essence the scenario described above. As illustrated in Fig. 1.12(a), as the pressure on packings is reduced, the points representing these packings in a $Z - n_m$ diagram approach the generalized isostaticity line [83]. Moreover, if the contacts at the mobility threshold are allowed to slip in analyzing the rotation-vibration dynamics, the density of states of packings close to the jamming threshold is strongly enhanced at low frequencies for *all* values of the friction coefficient μ — see Fig. 1.12(b). Moreover, as the pressure is increased to tune the packings away from the generalized isostaticity line, the crossover frequency ω^* in the density of states scales linearly with $\Delta Z = Z - Z^m_{\rm iso}$, *i.e.*, linearly with the distance from the generalized isostaticity line. This is the first confirmation of the robustness of the concepts reviewed above to frictional particles.

There are still several unresolved subtleties associated with the somewhat singular nature of the Coulomb threshold condition, but we refer for a discussion of these to [83]. Another interesting recent development [**?**] is that precursors to avalanches in simulations of tilting of piles of frictional spheres are found in the correlation properties of balls with low contact number.

1.3.3 Finite shear forces: nontrivial rheology in the sheared bubble model

So far we have only discussed static packings and their static and dynamic linear response. An important development of the last two years is that simulations of bubble models under finite shear stress or at a constant shear rate are probing the jamming phase diagram along the stress direction. The bubble model [20, 85] is essentially a soft-sphere model, enriched with viscous friction, *i.e.*, with dynamical terms proportional to the difference between the velocity of a bubble and that of each one it makes contact with. A particular attractive feature of such bubble model simulations with dynamic friction is the fact that the relevant reference frame for the static limit is the frictionless sphere or disc model, about which so much is known.

Olsson and Teitel [69] were the first to demonstrate that the rheological data for shear flows in such systems show very good data collapse close to the jamming point of the frictionless case. Fig. 1.13 shows a result from their simulations. In this particular plot, the effective viscosity $\eta = \sigma/\dot\gamma$ is plotted as a function of the shear stress σ imposed on the system; here $\dot\gamma$ is the shear rate. By scaling both quantities properly with the distance $\Delta\phi$ from the jamming density, there is very good data collapse both above and below the critical density. Moreover, at the jamming density, and close to the jamming density for large enough shear rates $\dot\gamma$, the data is consistent with a scaling

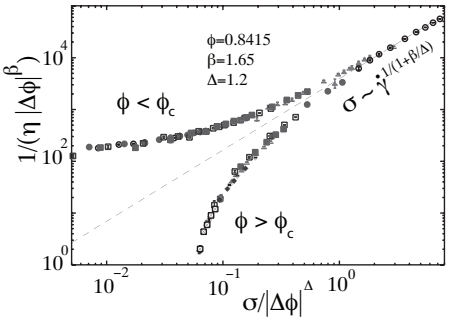

Fig. 1.13. Scaling plot of Olsson and Teitel [69] for simulations of the bubble model under shear. Plotted is a the viscosity $\eta = \sigma/\dot{\gamma}$, rescaled by the density, as a function of the applied shear stress σ, with $\dot{\gamma}$ the shear rate. The scaling collapse illustrates that close to the jamming point, nontrivial rheology occurs. Close to the jamming point, we have $\sigma \sim \dot{\gamma}^{1/(1+\beta/\Delta)} \simeq \dot{\gamma}^{0.4}$.

$\sigma \sim \dot{\gamma}^{0.4}$. The excitement in the field is due to the fact that this is one of the first examples of how a simple microscopic model leads to non-trivial rheological behavior at mesoscopic or macroscopic scales, and the fact that this is intimately related to the jamming scenario.

The more customary way to plot rheological data is to plot the stress σ as a function of the imposed shear rate $\dot{\gamma}$; this is how data like that of Fig. 1.13 are usually presented. At the time of writing this review, there is a lot of debate about the precise exponents [69,70,86–90], the existence of a quasistatic limit, the influence of the mean-field approximation employed in the simulations of [69], the question of whether there is a finite velocity correlation length which diverges at the jamming point, or one that is always of order the system size, etc. From our point of view, the essential question however is whether, just like in the static case, the exponents should be rational values which can be understood in terms of simple arguments based on our insight in the response of a marginal solid. To date, the answer to this question is unknown.

1.4 Real physical systems

As stated in the introduction, space limitations do not allow us pay tribute appropriately to the recent experimental developments that provide new impetus to the field. Some of these are reviewed in the chapters by Cipeletti and Weeks on colloids and by Dauchot, Durian and van Hecke on grains and foams. We wish to draw attention to a few additional points here.

1.4.1 Granular materials

Excited granular matter turns out to be an excellent model system to probe dynamical heterogeneities and the pair-correlation function $g(r)$ — think of

the experiments with discs shaken on a table [91, 92] or the ball bearing experiments [62, 63] discussed in section 1.2.7. Unfortunately, it is extremely difficult to probe the vibrational density of states with grains. The scaling of static properties like the contact number is also difficult to study experimentally: in experiments one will always have friction, whereas most of the clean theoretical scaling predictions are for frictionless spheres — as we have seen in section 1.3.2, with friction the behavior depends stongly on the way a packing is made, so it is not even clear whether clear scaling behavior should be expected in the experiments on photoelastic discs [22] aimed at measuring Z as a function of packing density (However, experiments using photoelastic discs have been very powerful in studying force-chain networks and correlations [93].) A powerful way to probe elasticity is to use ultrasound measurements, which, in agreement with what we have argued above, support a small G/B ratio in sand [94,95] and a sharp transition toward strong scattering [96] as the frequency increases. Another possibility which is being explored to probe the contact statistics and elastic moduli by using particles which swell when the humidity of the environment is changed [97]. Finally, experiments on avalanches are convenient for probing the length scales involved in failure and flows [98]. In particular the angle at which an avalanche starts depends strongly on the thickness of the granular layer. A model based on the stabilization of anomalous modes by the rough fixed boundary at the bottom of the granular layer is consistent with the observed dependence [99].

1.4.2 Emulsions and foams

It is important to stress here that some of the observations associated with the jamming approach — in particular, the scaling $\Delta Z \sim \sqrt{\Delta\phi}$ — already appeared in some form in the early work on bubbles and the bubble model [20, 85]. Moreover, it has become increasingly clear that wet foams are a very good experimental model system for jamming studies, since the friction is dynamic, not static. As a result, models of frictionless spheres or discs provide a reference frame to study the effect of shear. Indeed, recent experiments on sheared foams [100, 101] hold the promise for testing some of the predictions of the sheared bubble model that were discussed in section 1.3.3.

Another promising route is to use emulsions or foams. Here too, experiments from over a decade ago [102,103] already gave indications for deviations from the behavior expected for affine deformations. New, more-refined experiments, are called for. Emulsions have recently also been used to probe the structure of static packings [104].

1.4.3 Colloids

Soft colloids, such as foams, emulsions and particles made from poly(N-isopropyl acrylamide) microgels (NIPA particles) [105, 106], can be used to

study densities above the jamming transition. In aqueous solution, NIPA colloids swell substantially as the temperature is reduced only slightly. As a result, the packing fraction of the sample can be varied over a wide range with only a minimal change of temperature. The systems are thermal in that the particles are small enough (micron-sized) to exhibit significant Brownian motion. Thus, such systems are well-suited for studying jamming at a fixed non-zero temperature.

1.5 Connection with Glasses

In this section, we will describe some of the potential connections between the physics that appears at the jamming transition at point J and what happens in real molecular glass formers. There are several phenomena that appear ubiquitously in amorphous solids and glasses yet are quite different from what is found in ordinary crystals.

1.5.1 Properties of glasses to be considered

Density of low-temperature excitations and the Boson peak: There are many more low-frequency excitations in a glass than in a crystal. One of the hallmarks of glasses are the so-called anomalous low-temperature excitations. Since 1971 [107], it has been known that the specific heat, c_V of glasses varies approximately linearly with temperature rather than as T^3 as would be predicted by the Debye calculation where the low-frequency modes are long-wavelength planewaves [108]. At a somewhat higher frequency, above a frequency ω_{BP}, there is a dramatic excess of vibrational modes in glasses, known as the Boson peak [109]. That the Boson peak should be a ubiquitous property of amorphous solids is surprising since the underlying structure, which would normally determine the phonon spectrum in a crystal, is so different in different glasses. The linear specific heat is surprising since even disordered systems should have well-defined elastic moduli when averaged over large enough wavelengths. Therefore, at low enough frequencies, the modes should remain planewaves with a Debye spectrum. This linear specific heat has been ascribed to the quantum tunneling of groups of atoms between roughly equivalent structural configurations [110, 111] although these configurations have not been unambiguously identified.

Thermal conductivity: In a related vein, the heat transport in glasses is decidedly different from what it is in crystals [112]. At very low temperatures, the thermal conductivity, $\kappa \sim T^2$ rather than $\kappa \sim T^3$ as in crystals. At higher temperatures there is then a plateau region. Above the plateau there is a third regime where κ increases gently, $\kappa \sim T$. This behavior is surprisingly universal between different glasses yet there is no generally-accepted explanation of either of the higher-temperature regimes. The lowest-temperature region, where $\kappa \sim T^2$, has been modeled as the scattering of plane waves off the

localized tunneling systems used to explain the low-temperature linear term in the specific heat.

Failure under applied stress: When an amorphous solid is compressed or sheared sufficiently, it will start to fail. However, the failure often occurs in the form of rather localized rearrangement events rather than via a long-range catastrophic collapse [56, 58, 59]. Since the system goes unstable when the frequency of a mode reaches zero, it is possible to identify a rearrangement with the lowest-frequency mode just before the rearrangement [113]. However, ideally one would like to predict well in advance where failure will occur, even in large systems with many plane-wave-like modes at low frequencies.

Structure: In metallic and colloidal glasses, the structure has often been described in terms of sphere packings [114–116]. While this appears to be quite natural, there are certain features that have been related to the glassy structure that are not well understood. For example, the first peak in the pair distribution function, $g(r)$ is tall and sharp and there is a split second peak. Moreover, as the temperature is lowered in a supercooled liquid, there is no sign of the onset of rigidity in the static structure factor, $S(q)$; the first peak in $S(q)$ simply grows smoothly in height and decreases in width as the temperature is lowered through the glass transition temperature, T_g [117].

1.5.2 Relating the Jamming Paradigm to Glasses

Low-temperature excitations and the Boson peak in covalent glasses

Various theoretical approaches can reproduce a Boson peak and some of the features of the corresponding normal modes. They are based on disorder and generally connect the peak to an elastic instability, as in effective medium models [118,119], euclidian random matrix theory [120] or mode coupling [121]. However, the structural parameters controlling the peak are imposed by hand in these theories (amount of disorder in [119], density in [120] or structure factor in [121]). What aspects of the structure are the most relevant for the peak is unclear. Moreover, disorder cannot be a generic explanation for the Boson peak: silica has one of the largest peaks, but so do the corresponding crystals, the cristobalites, as shown in Fig. 1.14. It is sometimes argued that silica is a special case. The variational argument of section 1.2.3 shows that is not so: generically amorphous and crystalline elastic networks must have qualitatively similar low-frequency spectra if their coordination is identical. For example, a cubic lattice has a flat spectrum as does a random close packing of elastic particles. Thus coordination rather than positional disorder matters (but disorder in the spring stiffnesses obviously matters and can be incorporated in an improved variational argument [17]).

The variational argument of [24] has broad applications, as illustrated for silica and other tetrahedral networks following the analysis of [17, 122]. A particularity of silica or germanium oxide is the weak force constant associated with the rotation of two adjacent tetrahedra, in comparison with

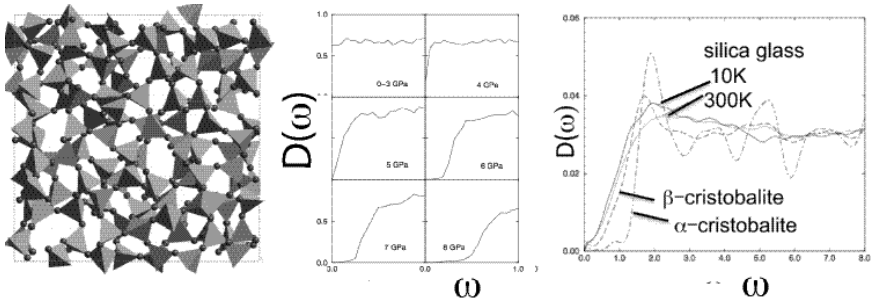

Fig. 1.14. Left: Configuration of amorphous silica as modeled by RUM: SiO_4 tetrahedra are connected by springs of finite stiffness at the joints, which can freely rotate [123]. Center: Density of states $D(\omega)$ for amorphous silica configurations obtained at various pressure within the RUM approximation. At low-pressure, there are only tetrahedra, and $D(\omega)$ is essentially flat. As the pressure increases 5-fold coordinated Silicon atoms become more and more numerous, and $D(\omega)$ erodes at low-frequency due to increased coordination, very much like in sphere packings [124]. Right: Computations of $D(\omega)$ for atomic models of silica. Silica glass, β-cristobalite and α-cristobalite all present a plateau above 1 Thz, the Boson peak frequency [123].

deforming the tetrahedra themselves. This suggests modeling silica as an assembly of stiff tetrahedra connected by flexible joints, the RUM model [123], as sketched in Fig. 1.14. When this approximation is used on configurations obtained at various pressures to compute the vibrational spectrum, one finds a remarkable similarity between silica and particles near jamming as illustrated in Fig. 1.14. The cause is identical: at reasonable pressures, silica is made of tetrahedra, and 5-fold defects are extremely rare. If joints are flexible, a tetrahedral network is isostatic (there are 6 degrees of freedom per tetrahedron, and 3 constraints per joint, and twice as many joints than tetrahedra) and must have a flat density of states, as observed. For real silica, the rotation of the joints has a finite stiffness, which must shift the anomalous modes forming the plateau by some frequency scale Δ. Using *ab initio* computation of the joint-bending force constant, and the molecular weight of silica one estimates $\Delta = 1.4Thz$. Empirically the density of states of silica indeed has a plateau above approximatively 1 Thz, as expected. This is shown in Fig. 1.14 for numerical simulations. This argument also applies to germanium oxide. For amorphous silicon, the bending force constant of the joints is comparable to the other interactions, since they correspond to the same covalent bond, and one therefore does not expect a Boson peak at low frequency; indeed in this material the Boson peak is nearly non-existent. Ref. [60] extends these arguments to other covalent networks.

Low-temperature excitations and the Boson peak in molecular glasses

We can make progress in understanding the excess number of low-frequency excitations in molecular glasses by recalling some of the properties of solids near the jamming transition. At point J, the jamming transition for frictionless

repulsive spheres, the density of states has a plateau all the way down to zero frequency. Upon compression, the plateau persists only down to a lower cutoff frequency, ω^* [5, 11] [Figs. 1.2 and 1.3(b)] as explained in [24]. Below that frequency, the normal modes are weakly scattered plane waves while above it they are strongly scattered [34,39,40,125] . This jump in $D(\omega)$ appears to be the counterpart to the dramatic increase in the number of vibrational modes that appear at the Boson peak in glasses [11, 17, 24, 126] .

In order to assert this correspondence more generally, we have ascertained that the physics dominating point J for repulsive spheres is also operative for other systems such as those with particles of non-spherical shape or with particles mediated by long-range and/or attractive interactions. To include such effects, we have studied several different models of glasses that can be analyzed in terms of their proximity to the jamming transition. We refer to section 1.3.1 on ellipsoids for a brief discussion of what happens when the particles are non-spherical — in essence, the results are consistent with the jamming scenario based on the analysis of frictionless spheres, though in a surprising and nontrivial way.

We have also studied models that were based on variants of the Lennard-Jones interactions between spheres. Such potentials allow attractive as well as long-range interactions so that the average coordination number can be arbitrarily large. Lennard-Jones potentials are more realistic models of molecular systems than the simple harmonic force law described above because the potential decays rapidly with inter-particle separation. Particles separated by even a slightly larger distance, interact much more weakly than those closer together.

We have shown [17, 126] that the onset of excess modes in these systems derives from the same variational-argument considerations that arise at point J for systems with finite-ranged repulsions. It can again be estimated by analyzing the vibrational energy originating from the excess contacts per particle over the minimum number needed for mechanical stability: $Z - Z_c$. The extra contacts can be divided into Z_1 strong contacts and the remaining $Z - Z_1$ weak ones. Strong contacts shift the energy cost of a mode that is initially zero in the isostatic limit to a nonzero value according to the variational argument outlined above, while weak contacts shift the energy simply by increasing the restoring force for displacements. The energy is then minimized to obtain the fraction of strong contacts. Even though these glasses have a high coordination number, most of the additional contacts can be considered to be weak.

These results are shown in Fig. 1.15 for two models. ω^* is the theoretical prediction for the onset frequency of excess modes based on the variational argument. The onset frequency determined from simulation is given by $\omega^\dagger$. The agreement between ω^* and $\omega^\dagger$ is very good. On the right-hand axis $\delta Z \equiv (Z_1 - Z_c)/Z_c$ is shown. Note that even though Z itself can be arbitrarily large, δZ remains small and does not get larger that 0.6. This is why these systems with high coordination can still be understood in terms of the physics of point J and isostaticity. Even though it may be impossible to reach the jamming

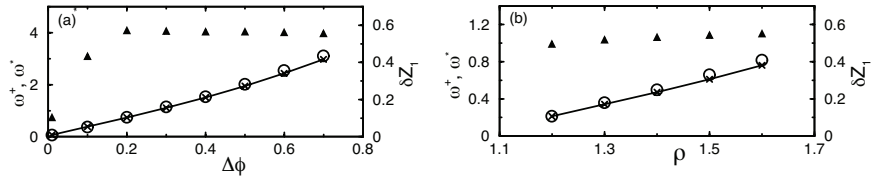

Fig. 1.15. Characteristic frequencies and fractional deviation from isostaticity for two three-dimensional systems based on Lennard-Jones potentials. Left panel shows data for repulsive Lennard-Jones bidisperse mixtures where only the repulsive part of the potential is included versus $\Delta\phi$, distance from the unjamming transition. Right panel shows data versus density, ρ, for a full Lennard-Jones potential with cutoff at $r = 2.5\sigma_{i,j}$ where $\sigma_{i,j}$ is the average diameter of particles i and j. On the left axis, $\omega^\dagger$ (open circles) is the onset frequency of the anomalous modes calculated from numerical simulations and the corresponding predictions for ω^* (crosses) based on a variational calculation. The agreement is very good. Lines are to guide the eye. On the right axis is the fractional deviation from isostaticity: $\delta Z \equiv (Z_1 - Z_c)/Z_c$ (solid triangles). Figure taken from [126]

transition itself for example because there are long range interactions or attraction (as in the Lennard-Jones system) the effects of the long-ranged part of the potential can be treated as a correction to the predominant effects of jamming.

Thermal conductivity: The thermal conductivity, κ, of a system near the jamming threshold has been calculated and captures well the thermal conductivity of silica glass above its plateau [39, 40]. Because the phonons are scattered so strongly by the disorder, phonon-phonon scattering is relatively unimportant so the thermal transport can be calculated within the harmonic approximation without recourse to the anharmonic properties of the modes. This is in strong contrast to the situation for crystals, where anharmonicity must be included to obtain a thermal conductivity that is not infinite. At the jamming threshold, the long-wavelength phonons that give rise to a diverging thermal conductivity in the harmonic limit are completely suppressed by the excess modes, since the density of vibrational states remains flat down to zero frequency. As a result, the thermal conductivity is finite even within the harmonic approximation at this special point. The thermal conductivity can be expressed in terms of the diffusivity, $d(\omega)$ (defined in section 1.2.6), and heat capacity, $C(\omega)$, of each mode:

$$\kappa(T) = \int_0^\infty D(\omega)\ C(\omega) d(\omega)\ d\omega\ , \tag{1.10}$$

In a weakly scattering system such as a crystal, $d(\omega) = c\ell(\omega)/3$ where c is the sound speed and $\ell(\omega)$ is the phonon mean-free path. As discussed in section 1.2.6, Fig. 1.8 shows that at the jamming transition $d(\omega)$ has a very simple shape: it is a plateau that extends from our lowest frequency up to the onset of the high-frequency localized states [39, 40], where $d(\omega)$ falls rapidly

to zero. The magnitude of the diffusivity in the plateau region, d_0, is small and scales as: $d_0 \sim \sigma^2\sqrt{\frac{k_{eff}}{M}}$ where $k_{eff} = \frac{\partial^2 V(r_{ij})}{\partial r_{ij}^2}$ is the effective spring constant of the system that scales as the bulk modulus, B. Effective medium theory suggests that these results hold more generally for weakly-coordinated disordered elastic networks [34].

Upon compression, the plateau region in $d(\omega)$ no longer extends down to zero frequency but only to a frequency that is proportional to ω^*. Thus all the modes above ω^* (excluding the truly localized modes at high frequency) have a nearly constant diffusivity. As we emphasized in the section on low-temperature excitations, ω^* obtained from the density of states corresponds to the frequency of the Boson peak. Here we find that this same frequency also is proportional to the onset of a region of flat diffusivity for thermal transport [39,40]. It is just such a region of constant diffusivity that was postulated by Kittel [127] to explain why the thermal conductivity of glasses has a weak, nearly linear, temperature dependence above the thermal-conductivity plateau. This is consistent with other evidence in glasses that the end of the plateau in $\kappa(T)$ corresponds to the Boson peak [107].

Failure under applied stress: As summarized in section 1.2.6, the vibrations of soft-sphere packings are quasi-localized near the onset of anomalous modes, ω^*: they have large displacements of relatively few particles while the rest of the mode has a very small amplitude. As the sample is compressed or sheared, it will eventually go unstable and rearrange into a new configuration. At zero temperature, this instability is governed by some quasi-localized mode in the system that goes "soft so that its frequency is pushed down until it reaches zero [113]. At this point, the sample moves into a new configuration. One cannot predict too much from the purely harmonic properties of a mode about what it will do when it is pushed to such a large amplitude that is goes unstable. However, at the very least one can say that at the point of instigation, the instability will initially have a very low participation ratio. This is consistent with the observation that when a glass fails due to pressure or shear stress, the failure tends to be highly localized in shear-transformation zones [58, 59]. So far, however, it has not been possible to identify shear-transformation zones unless they flip (unless a rearrangement occurs). The existence of many low-frequency quasilocalized modes with low energy barriers suggests that it may be possible to identify multiple shear-transformation zones from structural properties of the quasilocalized modes, and to predict which ones will flip *a priori*, even in large systems where there are many plane-wave-like modes at low frequencies.

Structure: At point J, the pair distribution function has many singular properties. In particular, we have shown that the first peak in $g(r)$ is a δ-function at the nearest neighbor distance, σ. The area under this δ-function is just the isostatic coordination number: $Z = 6$ in three dimensions. On the high side of this δ-function, $g(r)$ has a power-law decay: $g(r) \propto (r - \sigma)^{-0.5}$. Also, at the jamming transition, the second peak of $g(r)$ is split into what

appear to be two singular sub-peaks one at $r = \sqrt{3}\sigma$ and the other at $r = 2\sigma$. There is a divergent slope just below each subpeak and a step-function cutoff on its high side. The existence of a split second peak in $g(r)$ is a feature that is seen in many glasses, such as metallic and colloidal glasses. One can thus trace the origin of these subpeaks to the geometry at the jamming threshold. One can also ask why, as a supercooled liquid is cooled into the glassy state, there is no signature in the static structure factor, $S(q)$, which is how the structure of molecular glasses is determined from scattering experiments. At the jamming threshold, there are indeed clear signatures in the structure of a sample: these are the divergences just mentioned in $g(r)$. However, because $S(q)$ is the Fourier transform of $g(r)$, the divergences simply appear as slightly more pronounced oscillations in $S(q)$ out to very large wavevector.

1.6 Connection with Super-cooled liquids

The understanding of the glass transition remains one of the enduring mysteries of condensed matter physics. There is no doubt that the time scale for relaxation increases dramatically (faster than an Arrhenius law for what are called "fragile" glasses) as the temperature is lowered from the melt towards the glass transition temperature, T_g, but it is much less clear whether there are any static growing length scales that can be identified that accompany the slowing down [128,129]. However, as is well-documented in this book, there is a growing length scale associated with heterogeneities in the dynamics, which become increasingly collective as the viscosity increases. The origin of the super-Arrhenius increase of relaxation time with decreasing temperature (*i.e.* fragility) is controversial. Is it due to free-volume effects, thermal activation over energy barriers that grow with decreasing temperature, or some other type of cooperative motion?

1.6.1 Glass transition and soft modes in hard sphere liquids

Goldstein [130] has proposed that the slowing down of the dynamics is associated with the emergence of meta-stable states as a liquid is cooled. Such a roughening of the energy landscape is predicted by mean-field models of liquids and spins [131–134] at the so-called mode-coupling temperature T_{MCT}. However these theoretical approaches lead to a (non-observed) power-law divergence of the viscosity at T_{MCT}, and their interpretation in real space is unclear and actively studied [135,136]. Empirically, a direct validation of Goldstein scenario in liquids is difficult. Several numerical analysis [137–139] have claimed to observe a transition in the energy landscape at T_{MCT}, but in our opinion the interpretation of these results is disputable [1]. Another intriguing

[1] In these numerics, equilibrium configurations close to the configurations visited by the dynamics are analyzed. Their number of saddles (or unstable modes) is

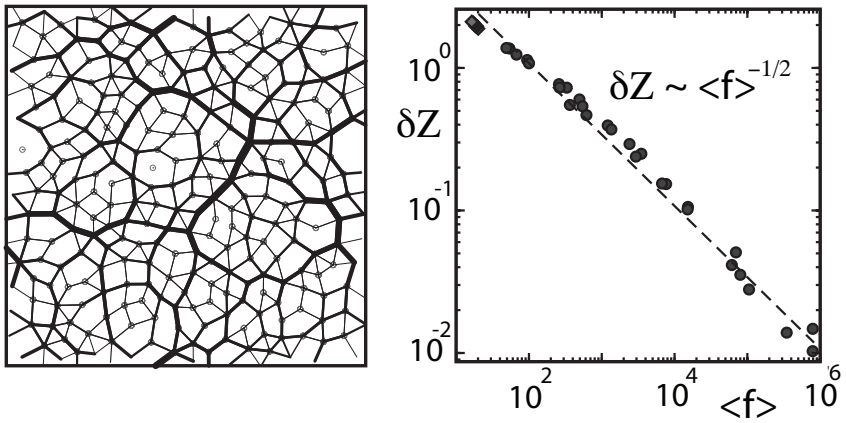

Fig. 1.16. Left: Illustration of the fact that the problem of hard elastic discs at finite temperature and density in the supercooled liquid or glass phase (in this case $\phi_c - \phi = 2 \cdot 10^{-4}\phi_c$), can, in between rearrangement events, be mapped onto the problem of a static packing with a logarithmic interaction potential [54, 140]. Essentially, particles experience a reduced free volume due to collisions with close neighbors, leading to an effective repulsive interaction. Thus particles exert a force on each other. The plot shows the average contact forces for 256 particles averaged over 10^5 collisions. The points represent the centers of the particles, and the thickness of the line is proportional to the force strength. Since in between rearrangement events the structure is stable, forces are balanced on each particle [54,140]. Right: ΔZ inferred from the coordination of the force network *vs.* average contact force $\langle f \rangle$, a measure of pressure. Measurements are made in the supercooled liquid (diamonds) and in the glass (circles). The observed coordination is well-captured by its minimal value $\Delta Z \sim \langle f \rangle^{-1/2}$ allowing mechanical stability, supporting that the glass is marginally stable [55].

aspect of Goldstein proposal is its application to hard spheres, where free volume rather than energy matters.

The connection between microscopic structure and vibrational spectrum established above directly supports that the emergence of meta-stable states

computed in function of the temperature, and it is argued that this quantity can be fitted by a curve that vanishes at a temperature T_{MCT}, defined here by fitting the dynamics as $\tau \sim (T - T_{MCT})^{-a}$, where τ is the α-relaxation time scale and a some exponent. From this observation it is stated that meta-stable states appear at T_{MCT}. However, this observation is precisely the behavior expected if meta-stable states had already appeared at larger temperature, implying that the dynamics is activated in the neighborhood of T_{MCT}. Indeed assuming activated dynamics, the number of saddles n_s reflects the probability that a region is in the process of rearranging (crossing a barrier), which occurs with a probability of order $1/\tau$. Thus one expects $n_s \sim 1/\tau$, which can be fitted with a vanishing quantity at T_{MCT} simply due to the definition of that temperature.

slows down the dynamics, and yields a geometrical interpretation of this phenomenon [55]. In order to see that, the theoretical description of anomalous modes and their associated length scales must be extended to finite temperature. An analogy between hard-sphere liquids and athermal elastic systems can be built [55, 140] in two steps: *(i)* on short time scales particles rattle rapidly but no large rearrangements occur. As illustrated in Fig. 1.16, a contact force network can be defined, following earlier work on granular matter [141], which represents the average force exchanged between particles. From such networks a coordination number is computed by counting the pairs of particles with a non-zero contact force. *(ii)* All the possible hard-sphere configurations associated with a given network can be summed up, leading to a computation of the free energy that can be expressed in terms of the mean positions of the particles. The effective interaction is found to be logarithmic. Expanding the free energy defines a dynamical matrix and vibrational modes that characterize the linear response of the mean particles positions to any imposed external forces within a meta-stable state.

The results on the vibrational spectra of athermal elastic networks apply to this case as well, and the stability criterion of Eq. (1.8) must be satisfied in any metastable configuration. For hard spheres, it can be written $\Delta Z > p^{-1/2} \sim h^{1/2}$ as the pressure p satisfies $p \sim 1/h \sim 1/\Delta\phi$, where h is the typical average gap among particles in contact. As illustrated in Fig. 1.16, the bound is approximatively saturated and the glass appears to have just enough contacts to maintain its stability. Marginal stability is a fundamental feature of the glass, generically foreign to crystals. It also occurs in some mean field spin models [132]. In hard spheres it implies the presence of anomalous modes near zero frequency and a curious behavior of the short-time dynamics, in particular a dependence on the mean-square particle displacements scaling as $\langle \delta R^2 \rangle \sim \Delta\phi^{3/2}$ rather than the $\Delta\phi^2$ dependence expected in a crystal [55]. Those predictions have been confirmed numerically [10, 54, 55].

Why is a hard sphere glass marginal? It has been argued [55] that this must be so if the viscosity increases very rapidly when meta-stable states appear in the free-energy landscape. In the $(\Delta Z, h)$ plane sketched in Fig. 1.17, Eq. (1.8) draws a line separating stable and unstable configurations. At equilibrium the mean value of ΔZ and h are well-defined functions of ϕ, and the corresponding curve is represented by the dashed line in Fig. 1.17. At low ϕ, gaps between particles are large and the configurations visited are unstable. As ϕ increases, the gaps decrease and configurations eventually become stable. This occurs at some ϕ_{onset} when the equilibrium line crosses the marginal-stability line. At larger ϕ, the dynamics becomes activated and intermittent, and the viscosity increases rapidly according to our hypothesis, so that on accessible time scales equilibrium cannot be reached deep in the regions where metastable states are present. As a consequence, the system falls out of equilibrium at some ϕ_0 larger than ϕ_{onset}. Configurations visited must therefore lie close to the marginal stability line, as represented by the dotted line in Fig. 1.17, since more stable, better-coordinated configurations cannot be reached dynamically.

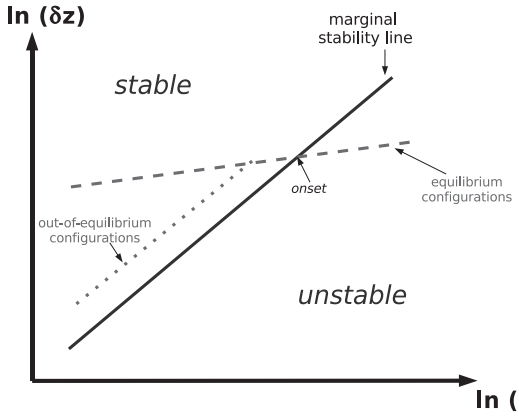

Fig. 1.17. Phase diagram for the stability of hard-sphere configurations, in the coordination δz *vs* average gap h plane. The marginal stability line delimits stable and unstable configurations. The dashed line correspond to equilibrium configurations for different ϕ. As ϕ increases, h decreases and the two lines eventually meet. This occurs at the onset packing fraction ϕ_{onset}, where the dynamics become activated and thus intermittent. At larger ϕ, viscosity increases sharply as configurations visited become more stable. For a finite quench rate the system eventually falls out of equilibrium at the glass transition packing fraction ϕ_0. More stable and more coordinated regions cannot be reached dynamically, and as ϕ is increased further, the system lives close to the marginal stability region, as indicated in the dotted line. The location of the out-of-equilibrium trajectory depends on the quench rate. In the limit of very rapid quench, the out-of-equilibrium line approaches the marginal stability line [55].

Further support for the view that the viscosity is governed by the presence of an elastic instability near ϕ_{onset} comes from the observation that the sudden rearrangements that relax the structure occur along its softest modes (both in the liquid and in the glass phase) [54], indicating that the lowest activation barriers lie in these directions, as illustrated in Fig. 1.18. Experiments in granular materials [142] and numerical observations of normal modes of the energy of inherent structures [56, 143, 144] reach similar conclusions. The normal modes of the free energy considered here are expected to correlate with the dynamics much better than those of the energy, and must be considered in particular when the interaction potential is strongly non-linear. The collective rearrangements involving a few tens of particles commonly seen in super-cooled liquids correspond mostly to a few modes [54], an effect even stronger in the glass phase. This analysis supports that the anomalous modes are the elementary objects to consider to describe activation, and that the collective aspect of rapid rearrangements is already present at the linear level in the structure of the modes.

This approach permits a quantitative study of activation, in particular to compute the fraction of the spectrum contributing to rearrangements. This

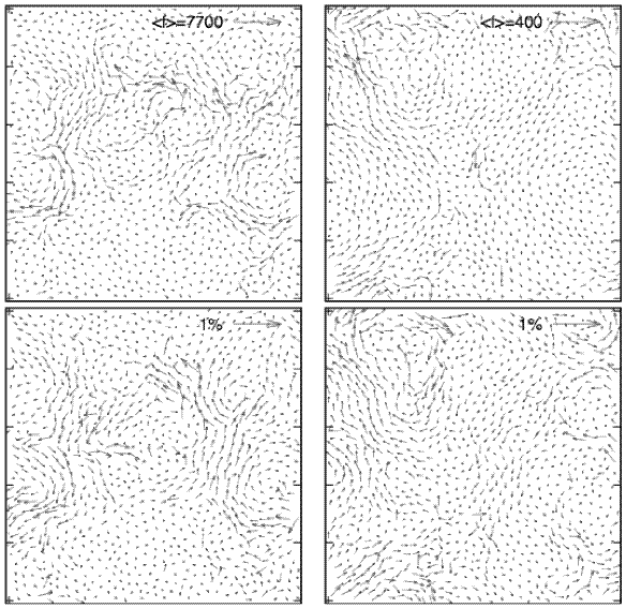

Fig. 1.18. Above: two examples of sudden rearrangements in the glass phase for different average contact force $\langle f \rangle$ for $N = 1024$ particles. Below: projection of these rearrangements on the 1% of the normal modes that contribute most to them, which systematically lie at the lowest frequencies [55]. This projection captures most of the displacement, indicating that a limited number of (collective) degrees of freedom are active during rearrangements.

quantity decreases rapidly with compression near the glass transition [54], implying that fewer and fewer degrees of freedom are relevant for the dynamics. This observed reduction of active degrees of freedom presumably mirrors the slowing down and increasingly collective aspect of the rapid rearrangements that relax the structure [145], but this has yet to be clarified.

Overall, the present approach furnishes a simple spatial picture for the slowing-down of the dynamics at intermediate viscosities: meta-stable states appear when the contact force network become sufficiently coordinated to resist the destabilizing effect of pressure. The localization for long times of an individual particle is thus not due to some specific properties of the cage formed by its neighbors, but has to do with the structure of the packing on a length l^* that can be large. Incidentally the concept of caging, commonly used to picture dynamical arrest, is misleading.

1.6.2 Models of soft finite range repulsions at finite temperature

By analyzing several models near the jamming threshold, some universal aspects of the slow-relaxation dynamics that appear in one asymptotic limit become apparent [146]. In particular, when the pressure, p, is small all the relaxation time data can be suitably plotted on a single master curve as a function of a single variable.

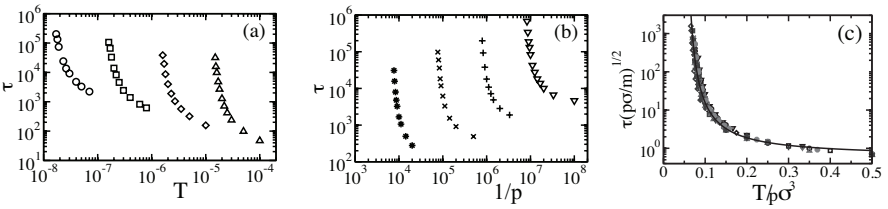

Fig. 1.19. Relaxation time, τ, versus temperature, T, (a) and versus inverse pressure, $1/p$, (b) for a system of spheres interacting via repulsive harmonic potentials. Panel (c) shows that all the relaxation time data for different potentials (harmonic, Hertzian and hard sphere) can be collapsed onto a single master curve. To get this data collapse, the relaxation time is non-dimensionalized by pressure and plotted versus $T/p\sigma^3$. Figure taken from [146].

The models considered here all have finite-range repulsions. For this study, thermal energy was included in the simulations, and the relaxation time τ of the system was measured by studying when the intermediate scattering function, $f(q,t)$ drops to e^{-1} of its initial value.

Normally in simulations of this type, one measures time in units of $\sigma\sqrt{m/\epsilon}$ where σ is the particle diameter, m is the mass of the particle, and ϵ is the energy scale of the potential. However, in order to produce a collapse onto a master curve, τ is non-dimensionalized in another way by using $\tau\sqrt{p\sigma/m}$. Plotting this quantity versus $T/(p\sigma^3)$ produces an excellent collapse of the data for several different potentials of interaction at all values of $T/(p\sigma^3)$ as long as the non-dimensionalized pressure, $p\sigma^3/\epsilon$ is sufficiently small [146]. This is shown in Fig. 1.19. This limit is satisfied at low pressures in soft-sphere systems and at any pressure for a hard-sphere system where $\epsilon \to \infty$. Fig. 1.19 shows that low-pressure soft-sphere data do indeed collapse with the hard-sphere result. In addition, Ref. [146] found that limiting hard-sphere behavior remains a good approximation up to higher values of $p\sigma^3/\epsilon$ as $T/(p\sigma^3)$ increases.

This data collapse has two important implications. First, it shows that at sufficiently low pressures the relaxation at the glass transition is a function of only a single variable. The molecular glass transition is, in this limit, equivalent to the hard-sphere colloidal glass transition. Second, Ref. [146] shows that there are systematic deviations from this universal behavior at larger values of the second control parameter: $p\sigma^3/\epsilon$. This demonstrates that there are at least two distinct physical processes that enter to produce glassy dynamics. What is important is that they can be cleanly separated, so that for sufficiently small $p\sigma^3/\epsilon$, the rescaled relaxation time is only a function of a single variable, $T/(p\sigma^3)$. Note that the existence of such a scaling function still does not tell us whether the rescaled relaxation time diverges at $T/(p\sigma^3) > 0$, implying that a thermodynamic glass transition exists, or at $T/(p\sigma^3) = 0$, implying that the glass transition is an isostatic jamming transition.

In order to understand the consequences of this result for molecular liquids, we must first understand the corrections to the leading hard-sphere behavior when we slowly increase $p\sigma^3/\epsilon$. These studies, have been done for repulsive spheres near the jamming threshold. However, molecular liquids typically have attractions and are at much higher densities than those considered here. To make the correspondence more general, we would have to push these systems farther from the jamming threshold. Nevertheless, this result shows how certain aspects of jamming, inherent in the hard-sphere liquid, are important for glass-forming liquids generally. As we have shown, at least one other distinct contribution to the relaxation must also be considered as the pressure is increased.

As one increases $p\sigma^3/\epsilon$, there are corrections to the leading hard-sphere behavior. It has been argued that these corrections can be collapsed onto a single curve by rescaling the pressure by some factor that varies with packing fraction [147].

1.7 Outlook to the future - A unifying concept

The vibrational spectrum of crystals consists of plane waves and leads to a description in terms of linear elasticity. In those systems, one can compute the non-linearities of the excitations and how they scatter from defects. Such a systematic description is lacking in amorphous solids. Various properties, such as thermal transport, force propagation, the vibrational spectrum and resistance to flow present phenomena that are not satisfactorily understood. An inherent difficulty in understanding these phenomena is that they are often governed by processes that occur on small length scales, of the order of a few particle sizes.

The discovery that the jamming threshold of athermal idealized spheres exhibits many properties of a critical point [5] changes this state of affairs, as it enables one to separate the length scale on which disorder matters from the molecular scale. This has led to the realization that the spectrum of amorphous solids is characterized by a crossover, distinct from Anderson localization, above which modes are extended but not plane-wave-like, and that the characteristic length at which this crossover occurs is decoupled from the molecular length. The corresponding excitations, the anomalous modes, allow one to understand several seemingly disparate anomalies in glasses and granular materials in a coherent fashion. The picture advanced in this review suggests that (1) the length scale l^* corresponding to the crossover characterizes force propagation in granular packings [26, 27], (2) the frequency scale of the crossover corresponds to that of the boson peak in glasses [11, 17, 24, 126], (3) the low-energy diffusivity of the modes above the crossover is responsible for the mild linear increase of the thermal conductivity with temperature above the plateau in glasses [34,39,40], (4) at least for colloidal glasses, the microscopic structure is marginally stable toward anomalous modes [55,140], (5)

the modes appear to govern structural rearrangements in liquids at least in the viscosity range that can be probed numerically [54–56]and (6) the structure of the modes corresponds to that of structural arrangements in amorphous solids under mechanical load [44, 148]. At the linear level those excitations and their consequences are now becoming rather well-understood theoretically for sphere packings, with the notable exception of *(i)* the observed quasi-localization of the lowest-frequency anomalous modes [44, 45] and *(ii)* the apparently fractal statistics of force propagation below the cut-off length ℓ^* above which continuum elasticity applies.

The jamming community is now beginning to study the non-linearities coupling these excitations. Much would be gained from such knowledge. On the one hand, it is possible that the lowest-frequency anomalous modes are related to two-level systems, which have been proposed on phenomenological grounds to explain transport and specific heat anomalies at sub-Kelvin temperatures. Despite decades of research, the spatial nature of two-level systems has remained elusive. If there is indeed a connection between the highly anharmonic, low-frequency, quasilocalized modes and two-level systems, then the energy barrier separating the two levels should vanish as the isostatic jamming transition is approached. On the other hand, since the low-frequency modes are involved in irreversible rearrangements, understanding their non-linearity is presumably essential for a microscopic description of the flow of supercooled liquids, granular matter and foams.

An exciting recent development is the advent of experiments capable of studying the vibrational properties of systems near the jamming transition [62, 149–151]. In laboratory systems, particle motion is typically damped and the inter-particle potentials are not necessarily known; this has made it difficult to make direct comparisons between experimental results and numerical and theoretical predictions until now. These complications have recently been overcome [149,150], so experiments should soon be able to test the extent to which predictions for ideal spheres apply to real systems.

Acknowledgement

We would like to thank Carolina Brito, Giulio Biroli, Jean-Philippe Bouchaud, Ke Chen, Doug Durian, Wouter Ellenbroek, Jerry Gollub, Peter Harrowell, Tom Haxton, Silke Henkes, Heinrich Jaeger, Alexandre Kabla, Randy Kamien, Steve Langer, Haiyi Liang, Tom Lubensky, L. Mahadevan, Xiaoming Mao, Kerstin Nordstrom, Corey O'Hern, David Reichman, Leo Silbert, Anton Souslov, Brian Tighe, Vincenco Vitelli, Martin van Hecke, Tom Witten, Erik Woldhuis, Ning Xu, Arjun Yodh, Zorana Zeravcic, and Zexin Zhang for valuable discussions, input, criticism and collaborations.

In addition, funding from DOE via DE-FG02-03ER46088 (SRN) and DE-FG02-05ER46199 (AJL) as well as the NSF MRSEC program via DMR-0820054 (SRN) and DMR05-20020 (AJL) is gratefully acknowledged. AJL

and SRN both thank the Kavli Institute for Theoretical Physics, Santa Barbara, and AJL, SRN and MW thank the Aspen Center for Physics for their hospitality. WvS would also like to thank in particular Martin van Hecke for his help and support during the last few years, and FOM for its generous support over the years.

References

1. A.J. Liu, S.R. Nagel, Nature **396**, 21 (1998)
2. J.C. Phillips, J. Non-Cryst. Sol. **34**, 153 (1979)
3. H. He, M.F. Thorpe, Phys. Rev. Lett. **54**, 2107 (1985)
4. P. Boolchand, G. Lucovsky, J.C. Phillips, M.F. Thorpe, Phil. Mag. **85**, 3823 (2005)
5. C.S. O'Hern, L.E. Silbert, A.J. Liu, S.R. Nagel, Phys. Rev. E **68**, 011306 (2003)
6. B.D. Lubachevsky, F.H. Stillinger, J. Stat. Phys. **60**, 561 (1990)
7. K. Shundyak, M. van Hecke, W. van Saarloos, Phys. Rev. E **75**, 010301 (R) (2007)
8. L. Berthier, T.A. Witten, Europhys. Lett. **86**, 10001 (2009)
9. P. Chaudhuri, L. Berthier, S. Sastry, (2009)
10. R. Mari, F. Krzakala, J. Kurchan, Physical Review Letters **103**, 025701 (2009)
11. L.E. Silbert, A.J. Liu, S.R. Nagel, Phys. Rev. Lett. **95**, 098301 (2005)
12. S. Alexander, Physics Reports **296**, 65 (1998)
13. C.F. Moukarzel, Phys. Rev. Lett. **81**, 1634 (1998)
14. D.A. Head, A.V. Tkachenko, T.A. Witten, The European Physical Journal E: Soft Matter and Biological Physics (1), 99
15. A.V. Tkachenko, T.A. Witten, Phys. Rev. E **62**(2), 2510 (2000). DOI 10.1103/PhysRevE.62.2510
16. J.N. Roux, Phys. Rev. E **61**(6), 6802 (2000). DOI 10.1103/PhysRevE.61.6802
17. M. Wyart, Ann. Phys. Fr. **30**((3)), 1 (2005)
18. S. Torquato, T.M. Truskett, P.G. Debenedetti, Phys. Rev. Lett. **84**, 111 (2000)
19. S. Torquato, F.H. Stillinger, J. Phys. Chem. B **105**, 11849 (2001)
20. D. Durian, Phys. Rev. Lett. **75**, 4780 (1995)
21. C.S. O'Hern, S.A. Langer, A.J. Liu, S.R. Nagel, Phys. Rev. Lett. **88**(7), 075507 (2002). DOI 10.1103/PhysRevLett.88.075507
22. T. Majmudar, M. Sperl, S. Luding, R. Behringer, Phys. Rev. Lett. **98**, 058001 (2007)
23. M.F. Thorpe, J. Non-Cryst. Sol. **57**, 355 (1983)
24. M. Wyart, S.R. Nagel, T.A. Witten, Europhys. Lett. **72**, 486 (2005)
25. M. Wyart, L.E. Silbert, S.R. Nagel, T.A. Witten, Phys. Rev. E **72**, 051306 (2005)
26. W.G. Ellenbroek, E. Somfai, M. van Hecke, W. van Saarloos, Phys. Rev. Lett. **97**, 258001 (2006)
27. W. Ellenbroek, M. van Hecke, W. van Saarloos, Phys. Rev. E (to appear)
28. D.A. Head, Phys. Rev. E **72**(2), 021303 (2005). DOI 10.1103/PhysRevE.72.021303
29. I. Agnolin, J.N. Roux, Phys. Rev. E **76**(6), 061304 (2007). DOI 10.1103/PhysRevE.76.061304

30. D.J. Jacobs, M.F. Thorpe, Phys. Rev. Lett. **75**, 4051 (1995)
31. W.G. Ellenbroek, Z. Zeravcic, M. van Hecke, W. van Saarloos, Europhys. Lett. **87**, 34004 (2009)
32. X. Mao, N. Xu, T. Lubensky. arXiv: 0909.2616 (2009)
33. E.J. Garboczi, M.F. Thorpe, Phys. Rev. B **31**, 7276 (1985)
34. M. Wyart, EPL **89**(6), 64001 (2010). DOI 10.1209/0295-5075/89/64001. URL http://dx.doi.org/10.1209/0295-5075/89/64001
35. I. Goldhirsch, C. Goldenberg, Eur. Phys. J E **9**(3), 245 (2002)
36. C. Goldenberg, I. Goldhirsch, Phys. Rev. E **77**(4), 041303 (2008)
37. P. B.Allen, J.L. Feldman, Phys. Rev. Lett. **62**, 645 (1989)
38. P. B.Allen, J.L. Feldman, Phys. Rev. B **48**, 12581 (1989)
39. N. Xu, V. Vitelli, M. Wyart, A.J. Liu, S.R. Nagel, Phys. Rev. Lett. **102**, 038001 (2009)
40. V. Vitelli, N. Xu, M. Wyart, A.J. Liu, S.R. Nagel. Preprint (2009)
41. P. Soven, Phys. Rev. **178**, 1136 (1969)
42. G. Monaco, S. Mossa, Proceedings of the National Academy of Sciences **106**(40), 16907
43. N. Xu, V. Vitelli, M. Wyart, A.J. Liu, S.R. Nagel, Phys. Rev. Lett. **102**, 038001 (2009)
44. N. Xu, V. Vitelli, A.J. Liu, S.R. Nagel. arXiv: 0909.3701 (2009)
45. Z. Zeravcic, N. Xu, A.J. Liu, S.R. Nagel, W. van Saarloos, EPL **87**, 26001 (2009)
46. R. Biswas, A.M. Bouchard, W.A. Kamitakahara, G.S. Grest, C.M. Soukoulis, Phys. Rev. Lett. **60**, 2280 (1988)
47. J. Fabian, P.B. Allen, Phys. Rev. Lett. **79**, 1985 (1997)
48. S.N. Taraskin, S.R. Elliott, Phys. Rev. B **59**, 8572 (1999)
49. H. R.Schober, G. Ruocco, Phil. Mag. **84**, 1361 (2004)
50. U. Bucheanau, Y.M. Galperin, V.L. Gurevich, D.A. Parshin, M.A. Ramos, H.R. Schober, Phys. Rev. B **46**, 2798 (1992)
51. U. Buchenau, C. Pecharroman, R. Zorn, B. Frick, Phys. Rev. Lett. **77**, 659 (1996)
52. Y.G. Vainer, A.V. Naumov, M. Bauer, L. Kador, Phys. Rev. Lett. **97**, 185501 (2006)
53. H. R.Schober, C. Oligschleger, Phys. Rev. B **53**, 11469 (1996)
54. C. Brito, M. Wyart, J. Stat. Mech. Theory - Exp **2007**, L08003 (2007)
55. W.M. Brito, C, Jour. of Chem. Phys. **131**, 024504 (2009)
56. A. Widmer-Cooper, H. Perry, P. Harrowell, D.R. Reichman, Nature Phys. **4**, 711 (2009)
57. C.E. Maloney, A. Lemaitre, Phys. Rev. e **74**, 016118 (2006)
58. M.L. Falk, J.S. Langer, Phys. Rev. E **57**, 7192 (1998)
59. J.S. Langer, Phys. Rev. E **57**, 021502 (2008)
60. M. Wyart, H. Liang, A. Kabla, L. Mahadevan, Phys. Rev. Lett. **101**(21), 215501 (2008)
61. L.E. Silbert, A.J. Liu, S.R. Nagel, Phys. Rev. E **73**, 041304 (2006)
62. A.R. Abate, D.J. Durian, Phys. Rev. E **74**(3), 031308 (2006)
63. A.S. Keys, A.R. Abate, S.C. Glotzer, D.J. Durian, Nature Physics **3**, 260 (2007)
64. Z. Zhang, N. Xu, D.T.N. Chen, P. Yunker, A.M. Alsayed, K.B. Aptowicz, P. Habdas, A.J. Liu, S.R. Nagel, A.G. Yodh, Nature **459**, 230 (2009)
65. Z. Zhang, N. Xu, D.T.N. Chen, P. Yunker, A.M. Alsayed, K.B. Aptowicz, P. Habdas, A.J. Liu, S.R. Nagel, A.G. Yodh., Nature **459**, 230 (2009)

66. H. Jacquin, L. Berthier, (2009)
67. L.E. Silbert, A.J. Liu, S.R. Nagel, Phys. Rev. E **73**, 041304 (2006)
68. J.A. Drocco, M.B. Hastings, C.J. Olson Reichhardt, C. Reichardt, Phys. Rev. Lett. **95**, 088001 (2005)
69. P. Olsson, S. Teitel, Phys. Rev. Lett. **99**, 178001 (2007)
70. J.J.C. Remmers, E. Woldhuis, B.P. Tighe, M. van Hecke, W. van Saarloos. unpublished (2009)
71. C.S.O. M. Mailman, C. F. Schreck, B. Chakraborty, Phys. Rev. Lett. **102**, 255501 (2009)
72. A. Donev, I. Cisse, D. Sachs, E.A. Variano, F.H. Stillinger, R. Connelly, S. Torquato, P.M. Chaikin, Science **303**, 990 (2004)
73. A. Donev, R. Connelly, F.H. Stillinger, S. Torquato, Phys. Rev. E **75**, 051304 (2007)
74. S. Sacanna, L. Rossi, A. Wouterse, A.P. Philipse, J. of Phys. Cond. Matt. **19**, 6108 (2007)
75. A. Wouterse, S.R. Williams, A.P. Philipse, J. of Phys. Cond. Matt. **19**, 6215 (2007)
76. Z. Zeravcic, N. Xu, A.J. Liu, S.R. Nagel, W. van Saarloos, EPL **87**, 26001 (2009)
77. K.L. Johnson, *Contact Mechanics* (Cambridge University Press, 1985)
78. L.E. Silbert, D. Ertaş, G.S. Grest, T.C. Halsey, D. Levine, Phys. Rev. E **65**, 051307 (2002)
79. H.P. Zhang, H.A. Makse, Phys. Rev. E **72**, 011301 (2005)
80. E. Somfai, J.N. Roux, J.H. Snoeijer, M. van Hecke, W. van Saarloos, Phys. Rev. E **72**(2), 021301 (2005)
81. E. Somfai, M. van Hecke, W.G. Ellenbroek, K. Shundyak, W. van Saarloos, Phys. Rev. E **75**(2), 020301 (2007)
82. C. Song, P. Wang, H.A. Makse, Nature **453**, 629 (2008)
83. S. Henkes, M. van Hecke, W. van Saarloos. arXiv:0907.3451 (2009)
84. J.P. Bouchaud, in *Les Houches Session LXXVII*, ed. by J.L. Barrat, M. Feigelman, J. Kurchan, J. Dalibard (Springer, Heidelberg, 2004)
85. D. Durian, Phys. Rev. E **55**, 1739 (1997)
86. T. Hatano, Phys. Rev. E **79**, 050301(R) (2008)
87. T. Hatano. ArXiv 0804.0477 (2008)
88. T. Hatano, J. Phys. Soc. Jpn. **77**, 123002 (2008)
89. P. Olsson, S. Teitel. (private communication) (2009)
90. T. Haxton, *et al.* (private communication) (2009)
91. F. Lechenault, O. Dauchot, G. Biroli, J.P. Bouchaud, EPL **83**, 46003 (2008)
92. F. Lechenault, O. Dauchot, G. Biroli, J.P. Bouchaud, EPL **83**, 46002 (2008)
93. T.S. Majmudar, R.P. Behringer, Nature **435**, 1079 (2005)
94. L. Bonneau, B. Andreotti, E. Clément, Phys. Rev. Lett. **101**(11), 118001 (2008)
95. X. Jacob, V. Aleshin, V. Tournat, P. Leclaire, W. Lauriks, V.E. Gusev, Phys. Rev. Lett. **100**(15), 158003 (2008)
96. X. Jia, C. Caroli, B. Velicky, Phys. Rev. Lett. **82**(9), 1863 (1999)
97. X. Cheng, Phys. Rev. Lett. (2009)
98. F.Y. Pouliquen, O., Ann. Rev. Fluid Mech. **40**, 124 (2008)
99. M. Wyart, EPL **85**, 24003 (2009)
100. G. Katgert, M.E. Moebius, M. van Hecke, Phys. Rev. E **101**, 058301 (2009)
101. G. Katgert, A. Latka, M.E. Moebius, M. van Hecke, Phys. Rev. E **79**, 066318 (2009)

102. T.G. Mason, J. Bibette, D.A. Weitz, Phys. Rev. Lett. **75**, 2051 (1995)
103. A. Saint-Jalmes, D.J. Durian, J. Rheol. **43**, 1411 (1999)
104. M. Clusel, E.I. Corwin, Alexander, O.N. Siemens, J. Brujic, Nature **460**, 611 (2009)
105. B.R. Saunders, B. Vincent, Adv. Colloid Int. Sci. **80**, 1 (1999)
106. R. Pelton, Adv. Colloid Int. Sci. **85**, 1 (2000)
107. R.C. Zeller, R.O. Pohl, Phys. Rev. B **4**, 2029 (1971)
108. N.W. Ashcroft, N.D. Mermin, *Solid State Physics* (Brooks Cole, 1976)
109. A.P. Sokolov, U. Buchenau, W. Steffen, B. Frick, A. Wischnewski, Phys. Rev. B **52**, R9815 (1995)
110. P.W. Anderson, B.I. Halperin, C.M. Varma, Philos. Mag. **25**, 1 (1972)
111. W.A. Phillips, J. Low Temp. Phys. **7**, 351 (1972)
112. A.C. Anderson, in *Amorphous Solids, Low Temperature Properties*, ed. by W.A. Phillips (Springer, Berlin, 1981)
113. C.E. Maloney, A. Lemaître, Phys. Rev. E **74**(1), 016118 (2006)
114. J.L. Finney, Nature **266**, 309 (1977)
115. R.W. Cahn, Contemp. Phys **21**, 43 (1980)
116. R. Zallen, *Physics of Amorphous Solids* (Interscience, New York, 1998)
117. L.E. Busse, S.R. Nagel, Phys. Rev. Lett. **47**, 1848 (1981)
118. W. Schirmacher, G. Ruocco, T. Scopigno, Phys. Rev. Lett. **98**(2), 025501 (2007). DOI 10.1103/PhysRevLett.98.025501
119. W. schirmacher, EPL (Europhysics Letters) **73**(6), 892 (2006). URL http://stacks.iop.org/0295-5075/73/i=6/a=892
120. T.S. Grigera, V. Martín-Mayor, G. Parisi, P. Verrocchio, Phys. Rev. Lett. **87**(8), 085502 (2001). DOI 10.1103/PhysRevLett.87.085502
121. W. Götze, M.R. Mayr, Phys. Rev. E **61**(1), 587 (2000). DOI 10.1103/PhysRevE.61.587
122. M. Wyart, in *Rigidity and Boolchand Intermediate Phases in Nanomaterials*, ed. by M.P. M. Micoulaut (INOE Bucarest, Bucarest, 2009), pp. 159–177
123. K.O. Trachenko, M.T. Dove, M.J. Harris, V. Heine, Journal of Physics: Condensed Matter **12**, 8041 (2000)
124. K. Trachenko, M.T. Dove, V. Brazhkin, F.S. El'kin, Phys. Rev. Lett. **93**, 135502 (2004)
125. L.E. Silbert, A.J. Liu, S.R. Nagel, Phys. Rev. E **79**, 021308 (2009)
126. N. Xu, M. Wyart, A.J. Liu, S.R. Nagel, Phys. Rev. Lett. **98**, 175502 (2007)
127. C. Kittel, Phys. Rev. B **57**((3)), 972 (1949)
128. M.D. Ediger, C.A. Angell, S.R. Nagel, J. Phys. Chem. **100**, 13200 (1996)
129. P.G. Debenedetti, F.H. Stillinger, Nature **410**, 259 (2001)
130. M. Goldstein, Jour. of Chem. Phys. **51**, 3728 (1969)
131. M. Mezard, G. Parisi, Journal of Physics A: Mathematical and General **29**(20), 6515
132. J. Kurchan, L. Laloux, Journal of Physics A: Mathematical and General **29**, 1929 (1996)
133. T. Castellani, A. Cavagna, Journal of Statistical Mechanics: Theory and Experiment **2005**(05), P05012
134. G. Biroli, J.P. Bouchaud. The random first-order transition theory of glasses: a critical assessment (2009). URL http://www.citebase.org/abstract?id=oai:arXiv.org:0912.2542
135. S. Franz, A. Montanari, Journal of Physics A: Mathematical and Theoretical **40**(11), F251

136. G. Biroli, J.P. Bouchaud, K. Miyazaki, D.R. Reichman, Phys. Rev. Lett. **97**(19), 195701 (2006)
137. L. Angelani, R. Di Leonardo, G. Ruocco, A. Scala, F. Sciortino, Phys. Rev. Lett. **85**(25), 5356 (2000)
138. K. Broderix, K.K. Bhattacharya, A. Cavagna, A. Zippelius, I. Giardina, Phys. Rev. Lett. **85**(25), 5360 (2000)
139. T.S. Grigera, A. Cavagna, I. Giardina, G. Parisi, Phys. Rev. Lett. **88**(5), 055502 (2002)
140. C. Brito, M. Wyart, EPL **99**, 149 (2006)
141. A. Ferguson, B. Fisher, B. Chakraborty, EPL (Europhysics Letters) **66**, 277 (2004)
142. C. Brito, O. Dauchot, G. Biroli, J.P. Bouchaud. Elementary excitation modes in a granular glass above jamming (2009). URL http://www.citebase.org/abstract?id=oai:arXiv.org:1003.1529
143. H. Schober, C. Oligschleger, B. Laird,
144. A. Widmer-Cooper, H. Perry, P. Harrowell, D.R. Reichman, The Journal of Chemical Physics **131**(19), 194508 (2009)
145. R. Candelier, O. Dauchot, G. Biroli, ArXiv e-prints (2009)
146. N. Xu, T.K. Haxton, A.J. Liu, S.R. Nagel, Phys. Rev. Lett. **103**, 245701 (2009)
147. L. Berthier, T.A. Witten, Phys. Rev. E **80**, 021502 (2009)
148. L.M. Manning, A.J. Liu. private communication (2009)
149. A. Ghosh, V. Chikkadi, P. Schall, Kurchan, J., Bonn, D., (2009)
150. K. Chen, W. Ellenbroek, Z. Zhang, D.T.N. Chen, P. Yunker, S. Henkes, C. Brito, D. Dauchot, W. van Saarloos, A.J. Liu, A.G. Yodh, (2010)
151. M. Gardel. private communication (2009)